PHYSICAL REVIEW B VOLUME 25, NUMBER 8 15 APRIL 1982

Calculation of the dynamic response of Schottky barriers with a continuous distribution of gap states

J. David Cohen and David V. Lang
Bell Laboratories, Murray Hill, New Jersey 07974
(Received 30 June 1981)

A full numerical analysis has been developed of the thermal transient and ac dynamic response of a Schottky-barrier space-charge region for a semiconductor with an arbitrary continuous density of gap states $g(E)$. These techniques are applied specifically to a calculation of current and capacitance deep-level transient spectroscopy as well as complex admittance versus temperature. We illustrate our methods on a host of hypothetical examples with densities of states similar to those obtained from studies of crystalline and amorphous semiconductors. A detailed comparison is made between the usual discrete-level case for material with a large dominant dopant level and the case of a material with a large and continuous density of deep-gap states. We also discuss the case of spatially nonuniform material and consider the case of fairly insulating material for which the equilibrium Fermi level lies near midgap. The application of our methods to actual analysis of experimental data of amorphous Si-H alloys to obtain a detailed picture of $g(E)$ is given in an experimental companion paper.

I. INTRODUCTION

The use of capacitance measurements of the Schottky-barrier space-charge region to obtain information about gap states in semiconductors has been developed over the course of nearly two decades of research. The theory relating deep-trap levels in crystalline semiconductors to capacitance as a function of voltage (C-V) as first discussed by Goodman,[1] or as a function of frequency, beginning with the early work of Sah and Reddi,[2] was developed in great detail by Senechal and Basinski,[3] Roberts and Crowell,[4] and Losee.[5] Losee, in particular, presented a very general treatment of the effects of gap states on the measured complex admittance of Schottky-barrier diodes as a function of frequency and temperature. Over the same period of time, dynamic thermally stimulated relaxation measurements on diode junctions were also developed beginning with early proposals to use capacitance-transient techniques by Williams[6] and by Furukara and Ishibashi.[7] Later developments include measurements of thermally stimulated currents (TSC) or capacitance (TSCAP),[8] and deep-level transient spectroscopy (DLTS).[9] These latter techniques have had considerable success identifying and studying the dynamic response of deep-gap states in crystals.

Recently the use of many of these techniques has been applied to the study of deep states in hydrogenated amorphous silicon (a-Si:H). Admittance measurements, first in the form of C-V and later as a function of frequency and temperature have been made on a-Si:H Schottky-barrier or metal-oxide–semiconductor (MOS) structures. A brief evaluation of the results of this work is given in the preceding paper.[10] Here we wish to note that analysis of these results until very recently followed along lines presented by Roberts and Crowell,[4] relevant for a low-frequency (or high-temperature) regime where all deep levels might respond to the applied ac voltage.[11,12] Lately, several analyses have been developed for variable frequency or temperature, notably by Snell *et al.*,[13] Viktorovitch and Moddel,[14] and Tiedje *et al.*[15] These analyses have taken one of two basic approaches. In one approach,[14,15] an equivalent-network analysis is used. This is perhaps the more appropriate analysis for fairly insulating (undoped) material where the time scales of measurement are comparable to the dielectric relaxation time. Snell *et al.*,[13] on the other hand, modify the low-frequency approach by imposing a frequency-dependent cutoff in the energy depth to which gap-state charge can respond.

In the last couple of years, a few attempts have also been made to apply thermal-transient techniques to a-Si:H,[16–18] including DLTS.[19–21] All

of the analyses given have been simple extensions of results known to be true for crystalline materials with low concentrations of deep levels (compared to net donor concentrations).

The difficulty in interpreting either the admittance or transient measurements has several aspects. The first is that transport itself is poorly understood in these materials. Second, there is considerable evidence that anomalous regions exist at or within 1000 Å of the surface of these films.[22–24] Finally, because deep concentrations are comparable to, or perhaps even exceed, shallow-state ("donor") concentrations, the usual analysis for transient effects may be greatly inaccurate due to the significant change in the depletion-region band bending that occurs during the emission of carriers from deep states. These latter two difficulties may exist, in some cases, even for crystalline materials.

The purpose of this paper is to present a detailed numerical analysis by which thermally stimulated transient effects in diode junctions, in particular DLTS, may be correctly interpreted for cases of an arbitrary density of gap states $g(E)$, or spatial variation $g(x,E)$. While the primary motivation for this work comes from a need to analyze DLTS spectra obtained on a-Si:H alloys, these techniques are also intended to find considerable utility in understanding crystalline data. Indeed, many of the assumptions inherent in our analysis have really been verified only for the case of crystals. Consequently, application of this analysis to a-Si:H should be considered in one sense as a test of many of those same properties for that material. Further discussion of the applicability of such assumptions to a-Si:H is presented in our experimental companion paper.[10]

In Sec. II of this paper, the basic theoretical development of our methods is presented. First we discuss the solution of Poisson's equation under steady-state conditions to give the correct band bending in the depletion region. While numerical analysis of this problem was previously treated by Spear *et al.*,[12] our methods are generally more suitable for cases of spatial variation within the space-charge region. A fast algorithm for solution of Poisson's equation is described which is crucial for the nonequilibrium, time evolution calculation. This discussion also includes the treatment of diodes in the deep depletion regime (large applied reverse bias).

We next consider the nonequilibrium evolution of the space-charge region following either a voltage pulse or laser pulse excitation. Such treatment is unique to the present work. The basic assumptions and theoretical framework for considering nearly all transient diode measurements for a semiconductor with nearly arbitrary $g(E)$ is set forth.

In the third part of this section, we adapt the analysis of Losee to obtain very general expressions for the ac response of a Schottky barrier or p^+n junction at any frequency ω, or temperature. These results are valid quite generally provided $1/\omega$ is longer than the dielectric relaxation time of the material. We obtain a solution to Losee's equations for the complex admittance in closed form which applies to cases where variations in $g(E)$ are small over the energy range of kT. This treatment extends somewhat the analysis of admittance in a-Si:H by previous authors.[13–15] A comparison of our methods and assumptions in this regard is discussed.

In the last part of Sec. II we consider specifically the case of capacitance and current DLTS. While our methods are readily applicable to TSC, TSCAP, or transient measurements at fixed temperatures, we restrict the illustration of our techniques primarily to DLTS and measurements of admittance versus temperature.

Section III presents calculations of DLTS and admittance for many classes of $g(E)$ and a variety of experimental parameters. At the beginning of this section we tabulate all of the assumptions essential to our methods of analysis and also list any additional assumptions used to illustrate the examples that follow. We then first consider the case of several nearly discrete levels both for its pedagogic value and to point out some less recognized aspects of DLTS measurements in crystals. Next we consider an example of a continuous but simple $g(E)$ and compare it in detail to the quasi-discrete case. Finally, we assemble a catalog of DLTS and admittance measurements for cases of $g(E)$ similar to many of those proposed for amorphous semiconductors. Since our methods are mostly numerical and not readily available to other workers, this detailed series of examples is intended as an aid to relate experimental DLTS and admittance measurements to an actual density of states. A method for obtaining a density of states $g(E)$ *beginning with* DLTS data is presented in the preceding paper.

Section IV concludes with some additional discussion of the assumptions used and the general applicability of this work. The extension of these calculations to explore as yet unobserved phe-

nomenon in amorphous semiconductors is considered briefly.

II. THEORETICAL DEVELOPMENT

A. General equations

If $\psi(x)$ and $\phi(x)$ denote the dc and ac band potentials, respectively, Poisson's equation becomes

$$\frac{d^2\psi}{dx^2}=\frac{\rho}{\epsilon},\quad \frac{d^2\phi}{dx^2}=\frac{\delta\rho}{\epsilon}\ , \tag{1}$$

where ρ and $\delta\rho$ are the dc and ac charge densities, respectively. We take the zero of energy for ψ to be the position of the conduction-band edge in the neutral bulk material. In thermal equilibrium the dc charge density is given by the usual integral over the density of states,

$$\rho(x)=q\int[f(E',E_F^0,T) -f(E',E_F^0-\psi(x),T)]g(E',x)dE'\ , \tag{2}$$

where E_F^0 is the position of the Fermi energy in the (neutral) bulk, f is the Fermi function, and q the electronic charge. If, as has often been customary,[11,12] we ignore any x dependence in $g(E)$ and consider this integral in the low-temperature limit we obtain a somewhat simpler expression:

$$\rho(\psi)=q\int_{E_F^0-\psi}^{E_F^0}g(E')dE'\ . \tag{3}$$

It is important at this point to explain our notation. We distinguish between the energy scale that relates to the physical sample and the energy scale that applies directly to the density of states. The symbols ψ, E_F, E_F^*, E_c, and E_v denote energies within the sample space-charge region while symbols with a zero superscript such as E_F^0, E_c^0, and E_v^0 are fixed with respect to $g(E)$. It is obvious that corresponding pairs of symbols differ only through the addition or subtraction of ψ. We shall further take E_c^0 as the zero of energy for $g(E)$ and define $\Delta E_F=E_c^0-E_F^0$ and $\Delta E_F^*=E_c-E_F^*$. Thus $E_F^0=-\Delta E_F$ and $E_c=\psi$.

Using Eq. (1) together with Eqs. (2) or (3) gives a straightforward integral differential for ψ. This situation is shown schematically in Fig. 1. Except for a few specific cases of $g(E)$,[25] this problem must be solved numerically. For small values of applied bias or for MOS structures the Fermi energy will extend through the barrier region[4] and

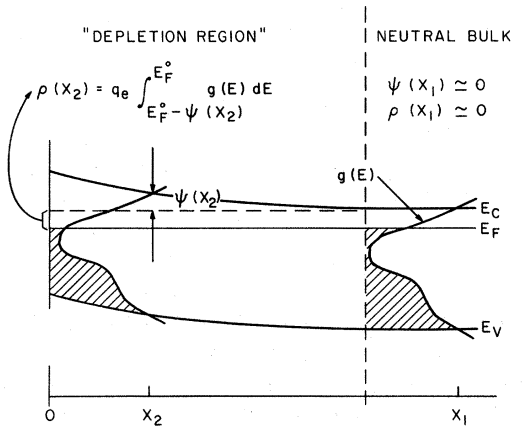

FIG. 1. Depletion region for equilibrium space-charge region for a material with a continuous density of gap states. The charge density is related to an integral involving the amount of band bending at each point x as indicated. The definition of various symbols is given in the text.

these equations are expected to remain valid. Such cases have been treated in the literature.[12]

For larger reverse bias applied to a Schottky barrier this picture must be modified. We will consider this situation in some detail since this discussion is also relevant to our treatment of time-dependent effects in Sec. II B. In general, occupation of states in the gap are dominated by majority- and minority-carrier emission and majority-carrier capture. The emission rate for electrons is usually written

$$e_n=\frac{1}{\tau_n}=\sigma_n\langle v_n\rangle N_c e^{-E/kT}\ , \tag{4}$$

where E is the energy *difference* between the particular localized gap state and the conduction-band edge, E_c^0, where carriers will move out of the depletion region in response to the electric field. The prefactor, $\sigma_n\langle v_n\rangle N_c\equiv\nu_n$ (where σ_n is the capture cross section for electrons into the state in question, $\langle v_n\rangle$ is the thermal velocity for electrons, and N_c is the occupation number for electrons in states above E_c^0), is readily derived by applying detailed balance to the case of thermal equilibrium. Indeed, thermal equilibrium requires that the capture rate *equal* emission rate at E_F. Hence, capture processes follow the same dependence on energy and temperature as Eq. (4). However, for capture the characteristic energy E is just the height of the conduction-band edge above the bulk Fermi level at the position x under consideration; i.e., $E=\Delta E_F+\psi(x)$. A similar expression applies to hole emission:

$$e_p=\frac{1}{\tau_p}=\nu_p e^{-E'/kT}, \tag{5}$$

where E' is the energy difference to the valence-band edge.

These expressions implicitly neglect *intrinsic* energy barriers to carrier capture which may exist if lattice relaxation plays a role in the capture or emission of localized states. This point is discussed in some detail in the experimental paper.[10] Simply put, such cases require a distinction be made between a "thermal equilibrium" energy scale and a "thermal emission" energy scale. To avoid undo complication, since for most cases of current interest these differences are found to be small experimentally, we shall ignore this distinction. Such refinements may be readily incorporated within the current framework as needed.

When a large reverse bias is applied to the Schottky diode, the potential barrier $\psi(x)$ depletes the region near the interface of free carriers from the bulk and the concentration of free carriers is wholly determined by leakage over the barrier at the metal interface. In simple isothermal diffusion theory[26] the current over a barrier of height ϕ_B is given by

$$J_0\simeq qN_c\mu_D\mathscr{E}_0\beta e^{-\phi_B/kT}, \tag{6}$$

where μ_D is the drift mobility, $\mathscr{E}_0$ is the electric field at the interface, $x=0$, and β is the transmission coefficient for majority carriers (which we shall assume are the electrons) across the barrier interface. For a transparent barrier, $\beta=1$. The use of diffusion theory or thermionic emission theory[27] is not crucial for our ultimate conclusions; however, for a low-mobility material such as *a*-Si:H Eq. (6) is probably somewhat more accurate. If n_c denotes the free-carrier concentration at a point x within the barrier region, current continuity then gives us

$$n_c=\frac{\mathscr{E}_0}{\mathscr{E}(x)}\beta N_c e^{-\phi_B/kT}. \tag{7}$$

The quasi-Fermi-level E_F^*, within the deep depletion region is found by simply setting the emission rate for electrons equal to the hole emission rate plus the electron-capture rate,

$$\nu_n e^{-\Delta E_F^*/kT}=\nu_p e^{-(E_g-\Delta E_F^*)/kT}+\sigma_n\langle v_n\rangle n_c,$$

or using Eq. (6),

$$e^{-\Delta E_F^*/kT}=\left[\beta\frac{\mathscr{E}_0}{\mathscr{E}(x)}\right]e^{-\phi_B/kT}+\left[\frac{\nu_p}{\nu_n}\right]e^{-(E_g-\Delta E_F^*)/kT}. \tag{8}$$

There are two obvious regimes: (1) If the first term on the right-hand side (rhs) is negligible, we get

$$\Delta E_F^*=\frac{E_g}{2}+\frac{kT}{2}\ln\left[\frac{\nu_n}{\nu_p}\right]. \tag{9}$$

This can occur either if the barrier height ϕ_B is significantly greater than half the band gap or for a small transmission coefficient β. Note that at room temperature, ΔE_F^* will lie within 0.1 eV of $E_g/2$ even if ν_n and ν_p differ by 3 orders of magnitude. (2) If the second term is negligible, corresponding to a small barrier, we obtain

$$\Delta E_F^*=\phi_B=kT\ln\left[\beta\frac{\mathscr{E}_0}{\mathscr{E}(x)}\right]. \tag{10}$$

Here, electronic levels will be empty to a depth below E_c roughly equal to the barrier height.

The general case is easily written down. Defining

$$\xi\equiv\left[\frac{\nu_n}{\nu_p}\right]^{1/2}\frac{\beta}{2}\frac{\mathscr{E}_0}{\mathscr{E}(x)}e^{(E_g/2-\phi_B)/kT},$$

we have

$$\Delta E_F^*=\frac{E_g}{2}+\frac{kT}{2}\ln\left[\frac{\nu_n}{\nu_p}\right]+kT\ln[-\xi+(\xi^2+1)^{1/2}]. \tag{11}$$

Equations (8) and (9) follow as special cases for $\xi<<1$ and $\xi>>1$, respectively. For the remainder of our discussion we will assume the former situation applies and take $\Delta E_F^*=E_g/2$.

In Fig. 2 we illustrate this situation. The quasi-Fermi-level follows the bulk Fermi energy into the tail region of the space-charge layer until it reaches an energy ΔE_F^* below E_c as given by Eq. (9). Thereafter it remains at a relatively constant level below E_c until very near the metal interface where, due to non-negligible free-hole concentration and hole capture, it moves away from $E_g/2$ to join E_F in the metal.

Our solution of the dc barrier problem is made numerically using a modification of the Noumerov

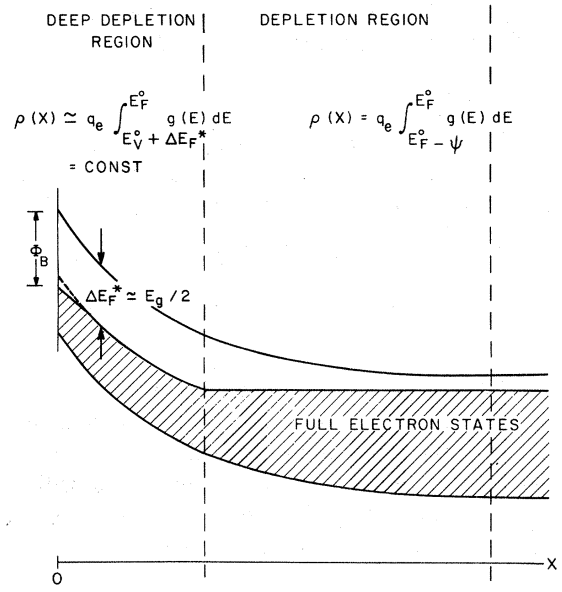

FIG. 2. Space-charge region in deep depletion. In the deep depletion region the charge density is approximately constant as determined by the position of the quasi-Fermi-energy. Parameters are defined in the text.

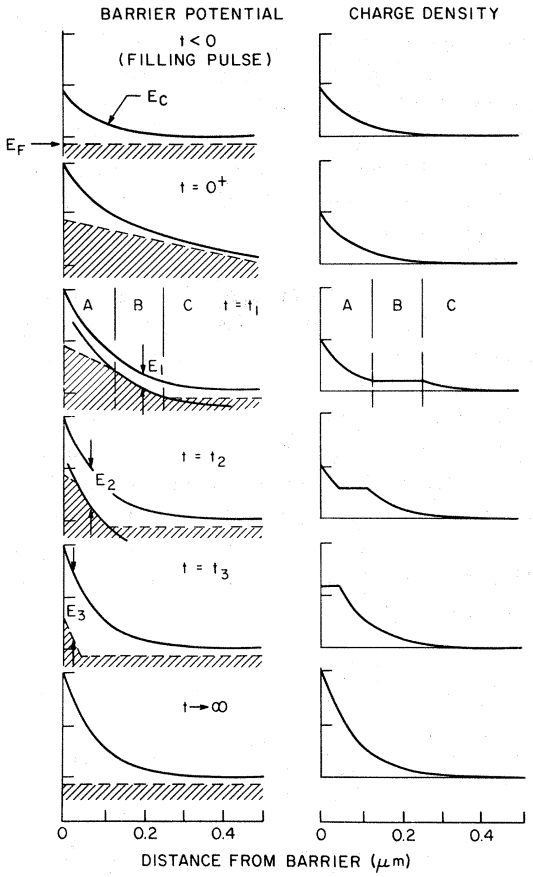

FIG. 3. Sequence of diagrams showing time evolution of space-charge region following an abrupt change of applied voltage. The curves for the barrier potential and charge density were obtained from a numerical calculation for a hypothetical material with a constant density of states $g(E)=10^{17}\ \mathrm{cm}^{-3}\mathrm{eV}^{-1}$. A detailed description and the definition of all parameters is found in the text.

technique.[28] Details of this approach applied to the diode space-charge layer are given in Appendix A. This method converges extremely rapidly for the equilibrium diode problem. Since this method specifically generates $\rho(x)$ rather than $\rho(\psi)$ (see, for example, Ref. 12) we are able to include trivially the case of spatially nonuniform structures. More importantly, the rapid convergence of the Noumerov technique is crucial to generate the nonequilibrium spectra described in the next section.

B. Nonequilibrium problem

1. Voltage pulse excitation

We wish to consider the evolution back to equilibrium of a Schottky-barrier diode in which a nonequilibrium occupation of gap states has been introduced. The simplest example occurs after a change of the applied diode bias voltage. This is the basis of "voltage pulse filling" in a DLTS or thermally stimulated evolution experiment.

Consider the sequence of diagrams shown for the *n*-type Schottky diode in Fig. 3. At $t=0$ the bias voltage is changed to a larger reverse value. Initially ($t=0^+$) the charge distribution is unchanged and the voltage change produces an additional constant field across the sample. At somewhat later times ($t=t_1$) three more or less distinct regions develop within the space-charge region. Near the diode interface (region *A*), the occupied states are too deep to have emitted any electrons. Thus the charge distribution is unchanged. Farther into the material (region *B*) charge has been emitted down to an energy depth $E_1 \propto \ln(t_1)$. Because this region is greatly depleted of free carriers, the charge distribution in this region is determined by emission processes alone; thus, the charge density is relatively constant. Finally, in the "tail" of the space-charge structure (region *C*) emission and capture rates are balanced; i.e., thermal equilibrium has been established. In this region the electron occupation can be described by the bulk Fermi en-

ergy.

As time progresses (see $t=t_3$), region A will eventually disappear as the system loses its memory of the initial conditions. Finally ($t\rightarrow\infty$), region B will disappear as the new equilibrium is obtained. However, for larger reverse bias, a region like B will persist at a characteristic quasi-Fermi-energy near midgap (see our previous discussion in Sec. II A).

The fact that such well-defined regions exist follows from the exponential dependence on energy of emission and capture rates as given by Eq. (4). This rapid variation with energy guarantees that the dividing line between regions A, B, and C (see diagram) will be sharp (to within Δx for a change of kT in ψ). It also assures that the demarcation between occupied and unoccupied electron states will be quite sharp. In region B the demarcation energy, i.e., the point of half occupancy ($n=\frac{1}{2}$), will be given by

$$E_1=kT\ln\left[\frac{\nu_n t_1}{\ln 2}\right]. \tag{12}$$

Figure 4 shows the variation of the occupation number n with energy in region B compared to a Fermi function with $E_F=E_1$ at $T=300$ K. We have chosen a value for the prefactor $\nu_n=2\times10^{13}$ which is representative of real materials. An evolution time of 10 μs has been used which gives a characteristic energy E_1 near 0.5 eV. We see that the demarcation between "empty" and "full" states is actually slightly sharper than a Fermi function

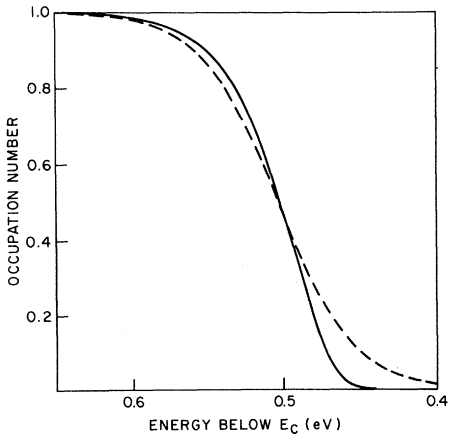

FIG. 4. Comparison of a $\Delta E_F=0.5$-eV Fermi function (dotted line) at room temperature with the function describing the electron state occupancy in region B of Fig. 3 (solid line) for $E_1=0.5$ eV also at room temperature.

at the same temperature. We denote the occupation function appropriate to region B by f^*:

$$f^*(E,E_1,T)=\exp(-e_n t_1), \tag{13}$$

with E_1 given by Eq. (12) and $e_n(E)$ by Eq. (4). This allows us to write the charge distribution in region B in a form analogous to Eq. (2):

$$\rho^*(E_1,T)=q\int[f(E',E_F^0,T)-f^*(E',E_1,T)]g(E')dE'. \tag{14}$$

The algorithm by which one computes a partially evolved space-charge region of characteristic energy E_1 is entirely straightforward. We denote the potential and charge distribution during the filling pulse by $\psi_0(x)$ and $\rho_0(x)$, respectively. We then numerically integrate Poisson's equation requiring

$$\rho=\begin{cases}\rho(x), & \psi(x)<E\\ \rho^*(E_1), & \psi(x)=>E_1>\psi_0(x)\\ \rho_0(x), & E_1=<\psi_0(x)\end{cases}$$

where $\rho=\rho(x)$ is given by Eq. (2) and $\rho=\rho^*(E_1)$ is from Eq. (14).

Figure 3 shows that the redistribution of gap state occupancy during the time evolution of the space charge can be rather complicated. For example, at roughly 0.25 μm from the interface the charge density first *increases* with time, then *decreases*. This occurs because electrons are first emitted far from the interface greatly increasing the positive charge density in the tail of the depletion region. At later times a positive charge builds up near the interface which necessarily shrinks the tail region in order to maintain a constant dipole moment of the Schottky-barrier space charge as mandated by Poisson's equation for a fixed bias.

For most cases of current interest we will be dealing with densities of states that do not vary appreciably over energies on the order of kT. It will therefore suffice to replace both the equilibrium (Fermi function) and nonequilibrium electron occupancy shown in Fig. 4 by step functions. This greatly simplifies the analysis. In particular this implies $\rho^*(E_1,T)=\rho^*(E_1)$. Thus we can consider that occupied gap states in region B have somehow been removed to an energy depth E_1 and ignore for the moment that this process takes place through *thermal* emission.

It is then possible to define the energy spectrum $R_r(E)$ for any characteristic response r of the

space-charge region. An obvious example of r would be the total barrier charge Q. We define

$$R_Q(E_1)=\frac{\partial}{\partial E}\int_0^\infty \rho(x,E)dx\Big|_{E=E_1},$$

where $\rho(x,E)$ is the charge density of the partially evolved space-charge region. The function $R_Q(E_1)$ thus denotes the change in total barrier charge as the energy depth from which states have evolved increases from E_1 to E_1+dE. For majority-carrier emission, this function becomes the basis for computing current transients. (For minority-carrier emission the correspondence is less straightforward. See the discussion under laser pulse excitation.)

An equally relevant example is the admittance. Here the energy spectrum for the capacitive response $R_C(E)$ forms the basis for computing the capacitance DLTS spectrum described in Sec. II D. In that section the utility of these energy-dependent response functions will become evident.

2. *Laser pulse excitation*

In order to significantly perturb the thermal equilibrium population of gap states below midgap an alternative to voltage pulse filling must be employed. The most obvious method is by light pulse excitation. Using Schottky barriers which have been made by depositing a sufficiently thin semitransparent metal layer on the semiconductor it is easily possible to obtain saturable laser pulse excitation with readily available sources.

The actual excitation mechanism involves both (1) the direct optical transitions between gap states and the conduction or valence bands, and (2) the capture into gap states of photoinduced free electrons and holes. Experimentally, the observation of a large laser-induced trap signal as the energy of incoming photons is increased above the optical gap suggests that the latter is the dominant mechanism. Immediately after the light pulse, therefore, one would expect a distribution of partially filled levels throughout the gap that is primarily determined by the relevant capture cross sections for electrons and holes.

The subsequent evolution of the space charge and potential in the barrier region is shown in Fig. 5. For this case there are two distinct regions: (1) the thermal equilibrium region C, and (2) an emission-rate-determined region B similar to region B for the voltage pulse filling. However, in this

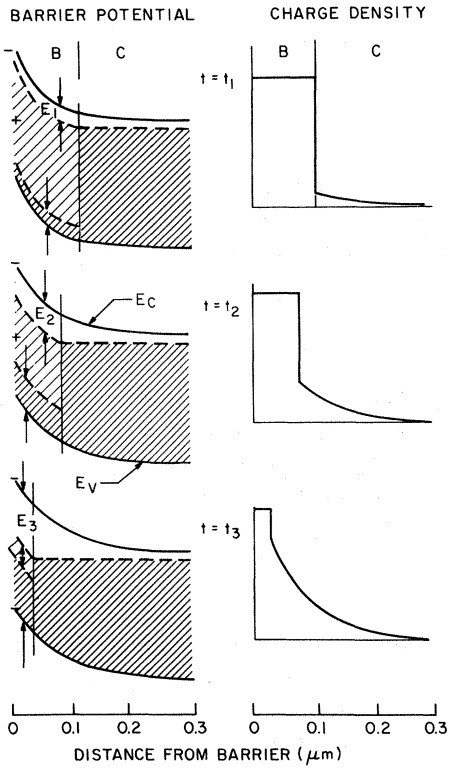

FIG. 5. Sequence of diagrams showing time evolution of space-charge region following a laser pulse excitation. The gap states for this material, again with $g(E)=\text{const}=10^{17}\ \text{cm}^{-3}\text{eV}^{-1}$, are assumed to be half occupied at $t=0$. A detailed description and definitions of parameters is given in the text.

case both electron and hole emission occur simultaneously so that after a time t_1 following the light pulse electrons have been emitted to a depth E_1^n from the conduction band given by Eq. (12) while hole emission has taken place to an energy E_1^p from the valence band

$$E_1^p=kT\ln\left[\frac{\nu_p(E_1^p)t_1}{\ln 2}\right]. \tag{15}$$

Note that the difference,

$$E_1^n-E_1^p=kT\ln[\nu_n(E_1^n)/\nu_p(E_1^p)],$$

is small even for ν_n and ν_p differing by an order of magnitude.

In principle the treatment of this case is identical to calculating the evolution following voltage pulse filling. We write the charge density in region B in a manner analogous to Eq. (14):

$$\rho^*(E_1^n,E_1^p)=q\int [f(E',E_F^0,T) - F^*(E',E_1^n,E_1^p,T)] \times g(E')dE' , \quad (16)$$

where $F^*(E',E_1^n,E_1^p,T)$ gives the net *electron* occupation in gap state levels and may be written in terms of the previous defined function f^*,

$$F^*=f^*(E,E_1^n,T) \times\{1-f^*(E,E_1^p,T)[1-\eta(E)]\} . \quad (17)$$

Here, E_1^n and E_1^p are energies measured from the conduction- and valence-band energies as given by Eqs. (12) and (15), respectively. The $t=0^+$ gap state occupation is given by the function $\eta(E)$. Poisson's equation may now be solved as a function of time in a manner exactly as in the previous case.

In practice, unlike the case of voltage pulse filling, experimental uncertainties force the adoption of two assumptions for comparison to actual experimental data. The first of these involves capture cross sections for minority carriers. Whereas capture rates for majority carriers are easily measurable (even to states involved in *minority*-carrier emission), minority-carrier capture rates are not so easily obtained. The second problem involves determining the post-light pulse occupation function, $\eta(E)$. Although saturation of the trap signal at photon energies just above the optical gap probably guarantees a uniform spatial distribution, the energy distribution is determined by the relative capture cross section for electrons and holes. A nonuniform and unknown $\eta(E)$ may therefore be impossible to deconvolve from an unknown $g(E)$. For the purpose of this discussion we shall always assume that $E_1^p=E_1^n$ and that $\eta(E)=$constant$=\frac{1}{2}$. However, experimentally this need not be true.

As before, by stepwise increases in E_1 to $E_g/2$ we may obtain the characteristic response functions $R(E)$. We noted for majority-carrier emission that we could compute current transients by evaluating the change in total barrier charge. This is *not* true if minority-carrier emission also takes place. Consider a Schottky barrier on n-type material and suppose emission of an electron causes the total barrier charge to increase by one unit. This amount of negative charge will then need to flow around the circuit to the metal side of the barrier to restore total charge neutrality to the junction. If, on the other hand, the emission of a hole causes the total barrier charge to decrease one unit, this positive charge will travel directly to the metal side of the junction and remain there. In general, because of displacement currents, the actual current observed in the external circuit is always a fraction of one unit for either electron or hole emission and depends on the spatial location of the emitted charge. For further discussion of this point, see Ref. 9. We shall denote by $R_{(Q)}(E)$ the energy spectrum of the response for the charge actually transported through the external circuit.

C. Admittance

In this section we develop expressions for the complex admittance applicable to both the equilibrium and nonequilibrium distribution of space charge within a Schottky-barrier (or p^+n) junction. We assume nondegenerate statistics and ignore any difference between thermal equilibrium and thermal emission energies. We further assume that mobilities are sufficiently high that dielectric response times are much faster than the timescales of interest. This assumption allows us to ignore details of transport.[10] For the present purpose we will assume the material itself to be spatially homogeneous. However, the analysis applies to specific classes of nonhomogeneous structures as discussed at the end of this section. The development of the relevant differential equations follows that given by Losee[5] and is given here for completeness and to define the notation.

Using the identity

$$\frac{d^2\psi}{dx^2}=\frac{1}{2}\left[\frac{d\psi}{dx}\right]^{-1}\left[\frac{d}{dx}\right]\left[\frac{d\psi}{dx}\right]^2 ,$$

we integrate Eq. (1) to obtain

$$H(\psi)\equiv\frac{2}{\epsilon}\int_0^{\psi}\rho(\psi')d\psi'=\left[\frac{d\psi}{dx}\right]^2 . \quad (18)$$

This is equivalent to a change of variables from x to ψ. Since we take the point $x=0$ to be the barrier interface, $\psi=0$ corresponds to a point far into the material (where $\rho=0$ follows from bulk neutrality). At $x=0$, $\psi=\phi_B-\Delta E_F-V_B\equiv V_S$, where ϕ_B is the metal-semiconductor height (see Fig. 2) and V_B is the applied bias voltage.

The usual dc capacitance C_0 is easily obtained from the charge per unit area at the interface, $\rho(V_S)$:

$$C_0=\frac{dQ}{dV}=\rho(V_S)H^{-1/2}(V_S)\ . \tag{19}$$

Now using the identity

$$\frac{d^2\phi}{dx^2}=\frac{d\phi}{d\psi}\frac{d^2\psi}{dx^2}+\frac{d^2\phi}{d\psi^2}\frac{d\psi}{dx}\ ,$$

we cast the ac part of the Eq. (1) into the form

$$\frac{d^2\phi}{dx^2}=\frac{\delta\rho}{\epsilon}=\frac{\rho(\psi)}{\epsilon}\left[\frac{d\phi}{d\psi}\right]+H(\psi)\frac{d^2\phi}{d\psi^2}\ , \tag{20}$$

where we have used Eq. (18). We define $F(\psi,\omega)$ as the small signal response of the ac charge,

$$\delta\rho=\phi F(\psi,\omega)\ . \tag{21}$$

If we further define

$$W(\psi)=\left[\frac{1}{\phi}\frac{d\phi}{d\psi}\right]^{-1}\ , \tag{22}$$

Eq. (14) assumes the form

$$\frac{dW}{d\psi}=1+\frac{\rho}{\epsilon H}W-\frac{F}{\epsilon H}W^2\ . \tag{23}$$

This is Losee's equation for the complex admittance. The connection with ac admittance Y follows by noting that the ac current density is $j=i\omega\sigma_{ac}$, where

$$\sigma_{ac}=-\epsilon\left[\frac{d\phi}{dx}\right]\Bigg|_{x=0}\ ,$$

is the ac surface charge density. Therefore,

$$Y(\omega)=\frac{j}{\phi}=-\omega\epsilon\left[\frac{1}{\phi}\frac{d\phi}{dx}\right]\Bigg|_{x=0}$$
$$=-\omega\epsilon\frac{d\psi}{dx}\left[\frac{1}{\phi}\frac{d\phi}{d\psi}\right]\Bigg|_{x=0}\ ,$$

where $Y(\omega)$ is the admittance per unit area. Using Eqs. (18) and (22), we obtain

$$Y(\omega)=i\omega\epsilon\frac{[H(\psi)]^{1/2}}{W(\psi)}\Bigg|_{\psi=V_S}\ . \tag{24}$$

Equation (23) is a first-order differential equation which is readily solved by numerical methods. The complex function W is directly related to the admittance of the junction via Eq. (24). The entire physics of capture and emission of carriers with regard to states in the gap in response to the applied ac voltage is contained within the complex function F.

Losee examines several examples for F applicable to the case of discrete levels. For the present case of interest, variations in $g(E)$ may be considered small over energies of order kT. In such a case we argue that the correct expression for F will be

$$F(\psi,\omega)=qg(E_F^0-\psi)(1+i\omega\tau)^{-1}\ , \tag{25}$$

where $1/\tau=e_n(\Delta E_F+\psi)$ as given by Eq. (4). To justify this, we first note that Eq. (25) has the right high-frequency characteristics since for large ψ, both $\delta\rho$ and F must vanish if levels are not able to respond on a timescale of $1/\omega$. Verification of Eq. (25) in the low-frequency regime follows immediately from Eq. (2) and the definition of F if we recall that

$$\frac{\partial f}{\partial\psi}=-\delta(E_F^0-\psi)\ ,$$

for functions varying slowly over kT.

In principle, then, the ac admittance can be directly obtained from Eqs. (23) and (24). In practice, however, having to solve Eq. (23) numerically is fairly cumbersome, particularly if we wish to calculate the evolution of the nonequilibrium diode admittance to obtain a complete energy spectrum of the capacitive response. Fortunately, an approximate analytic solution can be obtained which is valid at low temperatures and typically accurate to within a few percent at temperatures significantly above room temperature for most cases of interest. The details of this solution are presented in Appendix B along with a discussion of its general validity. In that analysis we define the position x_1 in the space-charge region measured from the barrier interface where the thermal emission rate is equal to the applied (angular) frequency of measurement:

$$\omega=\nu_n\exp\{-[\psi(x_1)+\Delta E_F]/kT\}\ . \tag{26}$$

Then, the imaginary and real parts of the admittance per unit area are given (approximately) by:

$$C=\epsilon\frac{\rho_1}{\epsilon H_1^{1/2}+x_1\rho_1}\ , \tag{27a}$$

$$\frac{G}{\omega}=kT\frac{\pi}{2}C^2\frac{H_1^{1/2}}{\rho_1^2}qg(E_F^0-\psi_1)\ , \tag{27b}$$

where H_1 and ρ_1 refer to the value of these functions at $\psi_1\equiv\psi(x_1)$. Note that C (as well as G) is a function of both ω and T via the relationship given by Eq. (26).

Equations (27) give the steady-state admittance at any applied bias as a function of temperature (or frequency). It is also readily demonstrated that nothing in the development of these equations pre-

cludes the applications of the methods to a nonequilibrium charge distribution of the type considered in the previous section *provided* this distribution does not change over the timescale of $1/\omega$. This follows from the fact that F then vanishes well within the "equilibrium region" (region C) of the charge distribution where ρ, H, and W are also well defined. Along the same lines, Eqs. (27) are correct even for cases of spatially nonuniform material provided the nonuniformity is confined between the barrier interface and $x=x_1$.

D. Deep-level transient spectroscopy

DLTS measurements are based on a well-defined algorithm which is easily expressed mathematically. If, for example, the capacitance of the junction at temperature T at a time t after the excitation is denoted as $C(t,T)$, the DLTS spectrum $S(T)$, which is measured using repetitive excitation while scanning temperature, is simply $S(T)=C(t_1,T)-C(t_2,T)$, where t_1 and t_2 are two experimentally chosen sampling times. A given pair of t_1 and t_2 determines the decay time τ_m (or rate window, $1/\tau_m$) to which the measurement is most sensitive,

$$\tau_m=\frac{t_2-t_1}{\ln(t_2/t_1)} . \tag{28}$$

In Sec. II B we introduced the energy-dependent function for the response r, $R_r(E)$, which is a valid means of expressing the evolution of the nonequilibrium space charge provided variations in $g(E)$ are small over energy widths of order kT. This function describes the variation per unit energy of the measured quantity r as gap state electrons respond at an energy depth E from the band edges. We now demonstrate that this function is nearly identical to the DLTS signal defined above.

For example, to obtain the capacitance DLTS signal from $R_C(E)$, we first take the Laplace transform of $R_C(E)$ to express the capacitance response in the time domain:

$$C(t,T)=\int R_C(E)\exp[-t/\tau(E)]dE , \tag{29}$$

where $\tau(E)$ is given by Eq. (4). For $\Delta t=t_2-t_1 \lesssim t_1$, we easily obtain, integrating by parts,

$$\begin{aligned} S(T)&=-\Delta t\frac{\partial}{\partial t}\int R_C(E)\exp[-t/\tau(E)]dE \\ &=-\frac{\Delta t}{\langle t\rangle}kT\int\frac{dR_C(E)}{dE} \\ &\quad\times\exp[-t/\tau(E)]dE , \end{aligned} \tag{30}$$

where $\langle t\rangle=(t_1+t_2)/2$. To a large extent the exponential factor merely truncates the integral at $E_T=kT\ln(\nu\langle t\rangle)$. Thus we obtain

$$S(T)\simeq-\frac{\Delta T}{\langle t\rangle}kTR_C(E_T) . \tag{31}$$

Apart from an overall minus sign, the essential difference between the DLTS signal and $R_C(E)$, is that the DLTS energy "window" increases linearly with temperature. This energy window gives rise to the factor of temperature in Eq. (31) and to a finite energy resolution $\delta E\sim E_T/10$.

Of course, the DLTS signal can be calculated directly in the time domain without invoking the slightly more restrictive assumptions needed to define $R_C(E)$. The primary reason for following the procedure we have is one of computational economy. Defining $R_C(E)$ allows us to recover both the time and temperature dependence of the barrier evolution process through one energy function. It also demonstrates that to a certain extent the DLTS signal is formally the Laplace transform of the transient signal.

In experimental practice one usually uses a double-boxcar integrator to obtain $S(T)$. In this case one replaces Eq. (30) with a slightly more complicated expression:

$$\begin{aligned} S(T)=&\frac{1}{\Delta t}\int_{t_1-\Delta t/2}^{t_1+\Delta t/2}C(t,T)dt \\ &-\frac{1}{\Delta t}\int_{t_2-\Delta t/2}^{t_2+\Delta t/2}C(t,T)dt , \end{aligned} \tag{32}$$

with $C(t,T)$ given by Eq. (29). Here Δt denotes the width the boxcar gates centered at t_1 and t_2. Note that this more general equation imposes no restrictions on the values of t_1, t_2, or Δt. Thus we use Eq. (32) rather than Eqs. (30) or (31) to compute actual DLTS spectra in Ref. 10.

For current DLTS, with a response energy function $R_Q(E)$ defined in Sec. II, a slightly different expression is obtained because it is the time derivative of the change in charge that is actually measured:

$$\begin{aligned} S(T)&=\frac{1}{\Delta T}\int_{t_1-\Delta t/2}^{t_1+\Delta t/2}\frac{\partial F(t,T)}{\partial t}dt-\frac{1}{\Delta t}\int_{t_2-\Delta t/2}^{t_2+\Delta t/2}\frac{\partial F(t,T)}{\partial t}dt \\ &=-\frac{1}{\Delta t}[F(t_1+\Delta t/2,T)-F(t_1-\Delta t/2,T)-F(t_2+\Delta t/2,T)+F(t_2-\Delta t/2,T)] , \end{aligned} \tag{33}$$

where

$$F(t,T)=\int R_Q(E)\exp[-t/\tau(E)]dE \ . \qquad (34)$$

One further point concerns capacitance DLTS for materials where the number of deep states is comparable to or exceeds the total number of shallow (or donor) levels. In such materials, the admittance itself varies markedly with temperature. In capacitance DLTS there are then two relevant timescales: that determined by the DLTS gate times τ_m, and that of the ac measurement frequency $1/\omega$. These spectra will therefore be characterized by an additional parameter

$$\gamma\equiv\frac{\ln(\nu/\omega)}{\ln(\nu\tau_m)} \ , \qquad (35)$$

where ν is the usual prefactor for thermal emission. This parameter is the ratio of the energy depth of the response on a timescale $1/\omega$ to that on a time scale τ_m; it is essentially independent of temperature. In Sec. III B we illustrate the effect of varying γ on the DLTS spectrum.

III. SPECIFIC CASE STUDIES

In this section we provide examples showing resulting admittance versus temperature plus voltage pulse and laser pulse DLTS spectra for several classes of $g(E)$. For this purpose we will adopt a variety of assumptions, some of which have been alluded to during the theoretical development in Sec. II. It is important to identify that these assumptions belong to one of two categories: (1) those which are essential to our basic formulation, and (2) those we adopt merely for simplicity of illustration or because in lieu of explicit evidence to the contrary they seem most likely to represent real materials. However, assumptions in this second category are readily modified within our theoretical framework. Included in the first category we assume:

(i) There is a well-defined band (or mobility) edge to which the emission from gap states takes place.

(ii) Time scales associated with the emission and capture processes of interest are much longer than dynamical limitations imposed by carrier transport (dielectric relaxation times).

(iii) We may ignore any retrapping of emitted carriers into deeper states within the depletion region. Note that retrapping into shallower states poses no particular problem since reemission will then occur on a much faster time scale than those relevant for the measurement.

(iv) Variations in $g(E)$ are small over energies of order kT.

(v) The semiconducting material is *laterally* homogeneous on a scale greater than the Debye screening length.

(vi) The usual set of conditions which define the usual Schottky-barrier problem under normal conditions[29] are valid. These include a well-defined barrier height, nondegenerate statistics, validity of quasi-Fermi-levels in describing steady-state behavior, absence of appreciable tunneling (except insofar as it merely serves to redefine an effective barrier), etc.

Within the second category we include:

(a) Thermal emission energies are assumed equal to thermal equilibrium energies. In case of doubt our energy scales should be interpreted as the former.

(b) The quasi-Fermi-energy in deep depletion is assumed to lie near midgap.

(c) All capture cross sections are assumed to be independent of energy and we further assume electron and hole emission prefactors are equal. (Where needed for illustration, we use the value $\nu=2\times10^{13}\ \mathrm{s}^{-1}$ obtained experimentally for *a*-Si:H.[10])

(d) The post-laser-pulse occupation function is taken to be a constant ($\eta=\frac{1}{2}$).

(e) We assume for the sake of simplicity that the position of the equilibrium Fermi energy and the magnitude of the energy gap are independent of temperature.

We now apply these assumption to some specific and hopefully relevant examples.

A. Quasidiscrete levels

Consider the case where $g(E)$ consists of a series of fairly sharply peaked levels, the most shallow of which is relatively large. This case is designed to simulate that of discrete levels in crystals with the concentration of deep levels much less than the net donor concentration.

Although the present formalism is less well suited to such a case, applying these techniques to this situation is valuable for a number of reasons. First of all, it verifies the validity of the numerical methods for a class of measurements that is presumably well understood. Second, it allows us to point out features in these measurements that are carried over to more general examples of $g(E)$

where the overall complexity of the spectra tends to obscure the interpretation. Finally, whereas the basic principles for interpreting discrete level spectra are known, there are many details of such spectra that are somewhat subtle in origin and not well recognized. These calculations therefore point out several aspects of discrete level spectra that have either not been previously discussed or discussed in only a qualitative manner.

The assumed density of states, shown in Fig. 6, consists of five Gaussian "trap" levels, each with a width parameter σ of 30 meV, and a total trap density N_T of 1×10^{15} cm^{-3}. The total shallow donor concentration N_s, assuming E_F to lie 50 meV below E_c, is 5×10^{16} cm^{-3} or 50 times N_T. This $g(E)$ produces a nearly parabolic band bending within the space-charge region which is affected only slightly by trap state occupation. The "width" of the depletion region, $W=(2\epsilon V_s/qN_s)^{1/2}$, is a reasonably well-defined concept.

In Fig. 7 the results of a 10-kHz admittance versus temperature measurements is simulated for a sample of 2×10^{-3} cm^2 area A and a silicon ($\epsilon=11.7$) dielectric constant. The applied bias plus barrier gives $V_s=5.5$ V ($V_B=-5$ V). Note the nearly constant value of capacitance at a value close to $\epsilon A/W=55$ pF. (The discrepancy is due to the contributions to the charge density due to the traps.) Two small capacitance "steps" of less than 1% of the total are observed at the temperatures where emission and capture rates for each of the two shallowest traps equal $1/\omega$. The real part of the admittance shows a corresponding peak in each case.

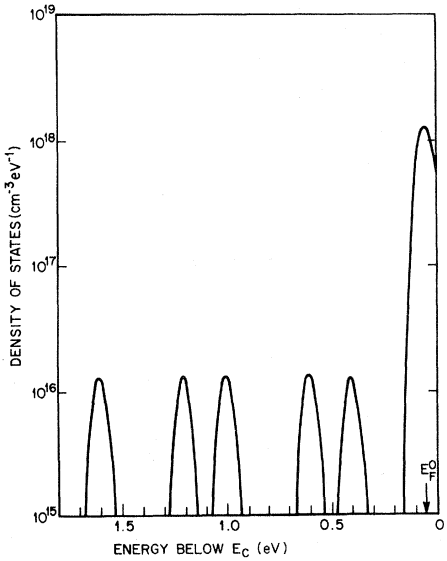

FIG. 6. Density of states showing five Gaussian "trap" levels, each with total integrated density 1×10^{15} cm^{-3}, plus shallow "donor" level corresponding to a net concentration of 5×10^{16} cm^{-3}. The position of the bulk Fermi energy is taken to be 50 meV below E_c and the gap energy is assumed to be 1.8 eV.

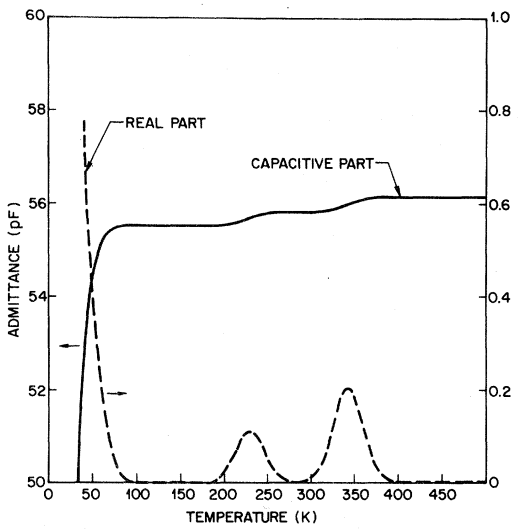

FIG. 7. Imaginary and real part of 10-kHz admittance obtained for density of states in Fig. 6 under 5-V reverse bias ($\phi_B=0.55$ eV). Note that the real part G/ω is also expressed in picofarads (pF) and is multiplied by a factor of 10 compared to the capacitive part (which is offset). The junction area A is taken to be 2×10^{-3} cm^2.

Figure 8 shows capacitance DLTS for the same bias voltage using a series of different filling voltages V_p from one volt above V_B to flat band. (Here, V_p denotes the value of the bias voltage *during* the filling pulse, not the pulse height.) Actually the spectra in Fig. 8 are the capacitance response energy spectra $R_C(E)$ as defined in Sec. II. Temperature-scan DLTS spectra may be obtained readily using Eqs. (31) or (32). The reason we prefer here to display $R_C(E)$, apart from its greater generality, is that the DLTS peak amplitudes for truly discrete levels are better compared to the integral of $R_C(E)$ over each trap peak which is independent of temperature, rather than $S(T)$. Thus, for a 2×10^{-3}-cm^2 sample, the *total* capacitance change ΔC_1 for the most shallow trap with V_p at flat band ($+0.5$ V) is 0.31 pF. The other curves may be scaled accordingly. Note that there is also an overall *sign* difference between $R_C(E)$ and the DLTS signal $S(T)$ as defined in Sec. II D.

It is interesting to compare these calculated re-

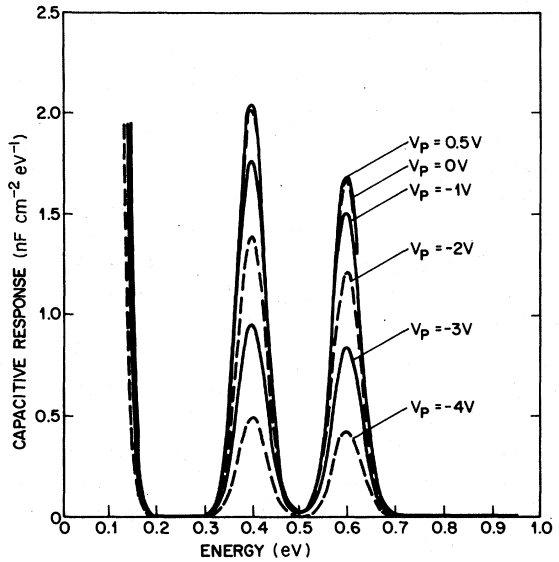

FIG. 8. Capacitive response energy spectrum $R_C(E)$ for the density of states of Fig. 6 under -5-V bias for a series of filling pulse voltages V_p. Here, V_p refers to the value of the applied bias during filling.

sults with the standard formulas used to estimate trap concentrations. In Fig. 8 we see the nearly linear increase of signal height with filling pulse voltage, which has been predicted.[9] The trap concentration usually is given by[9]

$$N_T = \frac{g\epsilon A^2 (N_S)^2}{C_0^3}\left[\frac{\partial(\Delta C)}{\partial V_p}\right], \tag{36}$$

where C_0 is the steady-state capacitance at the applied bias. For the two traps seen in the figure we obtain: $N_T(1)=7.4\times10^{14}$ cm^{-3} and $N_T(2)=6.5\times10^{14}$ cm^{-3}. The actual concentrations are 1×10^{15} cm^{-3}. These discrepancies can be understood if we realize that deep traps influence only a fraction of the total depletion width depending on where the trap level crosses the Fermi level as illustrated in Figure 9. Equation (36) applies accurately only in the limit of shallow traps or large bias voltage.

This point is further illustrated if we examine the dependence of the DLTS signal on bias voltage as shown in Fig. 10(a). In each case V_p is the flat-band voltage. The apparently complicated dependence on bias voltage is easily derived using principles well known from studying discrete trap levels in crystals. First of all, for $N_S >> N_T$, the total change in capacitance δC that occurs if N_T traps are emitted is

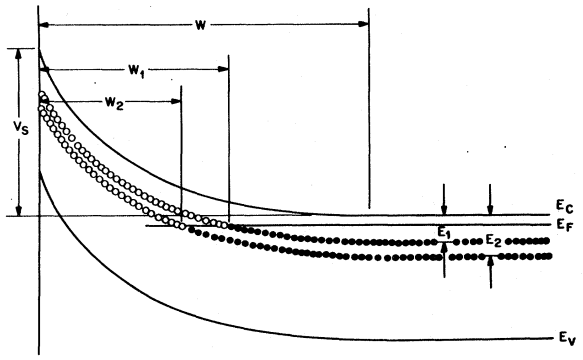

FIG. 9. Diagram defining the width W_n as the distance from the barrier interface where the trap level at E_n crosses the Fermi energy. The open and closed circles indicate traps empty or full, respectively.

$$\delta C = \delta\left[\epsilon A\left[\frac{qN}{2\epsilon V_S}\right]^{1/2}\right] = \tfrac{1}{2}C_0\frac{\delta N}{N}$$

or

$$\frac{N_T}{N_S} \simeq \frac{2\delta C}{C_0} . \tag{37}$$

However, this is again true only if trap emission occurs over the entire depletion width W. From Fig. 9, we define the distance at which each trap crosses the Fermi energy,

$$W_n \equiv W - [2\epsilon(E_n - \Delta E_F)/qN_S]^{1/2} . \tag{38}$$

We recall that for capacitance DLTS the sensitivity to emission of trapped charge increases linearly with the distance from the interface.[9] Hence the actual signal will be given by

$$\delta C_n = \frac{\int_0^{W_n} x\,dx}{\int_0^{W} x\,dx}\delta C_{\max} , \tag{39}$$

where $\delta C_{\max}$ is given by Eq. (37), or

$$\delta C_n = \frac{W_n^2}{W^2}\frac{N_T(n)}{N_S}\frac{C_0}{2} . \tag{40}$$

Using Eqs. (38) through (40), we list in Table I values for δC_n expected for the two traps seen in voltage pulse DLTS along with the total (integrated over energy) values obtained from Fig. 10(a). The close agreement demonstrates the accuracy of our numerical methods.

In Fig. 10(b) we show the corresponding DLTS spectra for thermally stimulated charge-transport measurements. Here the dependence on bias volt-

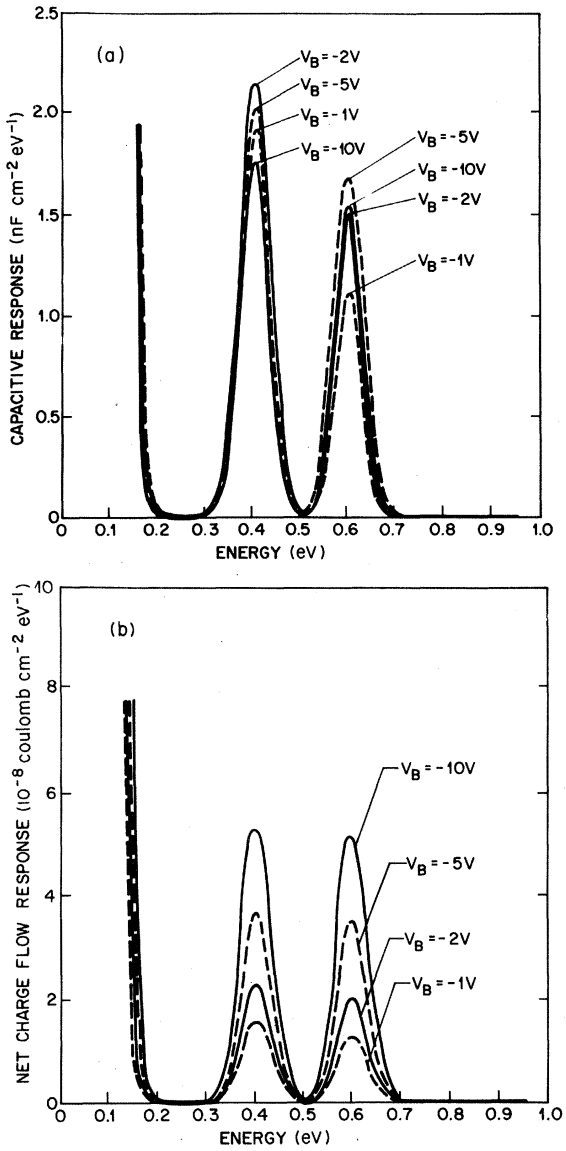

FIG. 10. (a) Capacitive response energy spectra $R_C(E)$ for $g(E)$ of Fig. 6 as a function of bias voltage. In each case the filling pulse voltage V_p is the flat-band voltage ($V_p=+0.5$ V). (b) Corresponding net charge flow energy spectra $R_Q(E)$ for the conditions described in (a).

age is much different from Fig. 10(a). This occurs because the sensitivity to majority carrier emission for current DLTS is *largest* at the barrier interface and decreases linearly to zero at the edge of the depletion region (due to cancellation from displacement currents).[9] The expected signal is

$$\frac{\delta Q^n}{A}=qN_T(n)\int_0^{W_n}(1-x/W)dx$$
$$=qN_T(n)W_n(1-W_n/2W)\,. \qquad (41)$$

A comparison between Eq. (41) and the numerical results in Fig. 10(b) are included in Table I.

Figures 11(a) and 11(b) show the energy spectra for the laser-pulse-induced capacitance and charge-transport response for variable V_B. Several interesting features in these spectra may be noted. For the capacitive response, as expected, electron and hole emission give rise to signals of different sign. The negative signals at 0.2 and 0.8 eV correspond to the traps 0.2 and 0.8 eV away from the valence band, respectively. The positive signal at 0.4 eV is the electron emitting trap at $E_c-0.4$ eV. At 0.6 eV there is near cancellation from two traps at 0.6 eV from valence and conduction bands, respectively. The magnitude of both electron and hole signals, as measured from the nonzero baseline, agrees with Eq. (40) if we divide by two to take the $\eta=\frac{1}{2}$ laser pulse filling factor into account.

In current DLTS, electron and hole emission produce signals of the same sign. Therefore, in Fig. 11(b) one sees four distinct peaks: the signals due to the traps 0.6 eV from the conduction and valence bands now add constructively. For electron emission the signal magnitudes obey Eq. (41) multiplied by $\eta(E)$. However, for hole emission we have the *opposite* spatial sensitivity (see discussion at end of Sec. II B). Therefore, for *minority carriers*,

$$\frac{\delta Q^n}{A}=qN_T(n)\frac{W_n^2}{2}\,. \qquad (42)$$

This agrees quite well with the numerical calculation.

One striking feature in Fig. 11(a) is the baseline behavior. This results from electron *capture* into partially occupied states in the tail region (region C of our discussion of Sec. II B) as free carriers from the bulk are able to penetrate the depletion layer. Such a process also manifests itself as the small *negative* current baseline that appears in Fig. 11(b). This is a somewhat surprising effect which can only occur when partially occupied states have been induced *below* the steady-state quasi-Fermi-level for majority carriers. The effect disappears as the emission process destroys the fractional occupation of these states.

The different spatial sensitivity for capacitance and current signals is most dramatically illustrated when spatially inhomogeneous materials are encountered. Suppose that within 500 Å of the metal interface a level exists which is 0.5 eV below E_c, has the same width as the five "bulk" levels but is

TABLE I. Comparison of the results of our numerical calculation for DLTS peak signals of different applied bias voltages with standard formulas for discrete level signals as explained in the text. This comparison is made for both the 0.4-eV (level 1) and 0.6-eV level (level 2) as shown in Fig. 6 for both capacitance (ΔC) and current transient (ΔQ) measurements. Note the good agreement between the numerical calculation and values given by the discrete level formulas.

	ΔC_1 (pF)		ΔC_2 (pF)		ΔQ_1 (10^{-9} C)		ΔQ_2 (10^{-2} C)	
V_s (V)	Eq. (39)	Numerical	Eq. (39)	Numerical	Eq. (40)	Numerical	Eq. (40)	Numerical
1.5	0.282	0.290	0.165	0.169	24.2	23.9	20.0	19.7
2.5	0.319	0.323	0.230	0.230	34.9	34.3	31.7	30.9
5.5	0.307	0.307	0.257	0.253	56.5	55.5	54.3	52.7
10.5	0.266	0.265	0.237	0.233	80.5	78.8	79.0	76.7

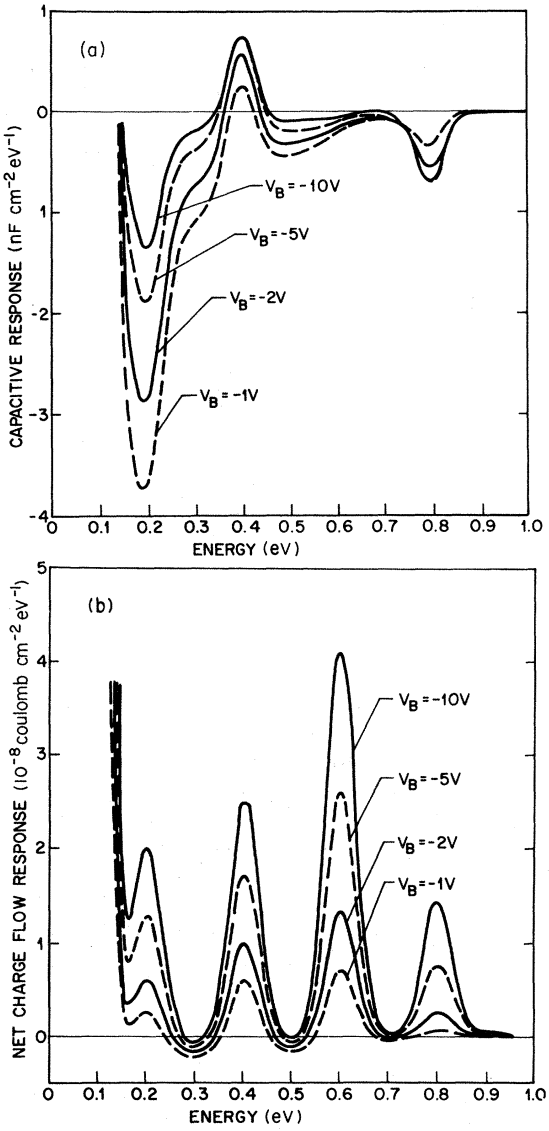

FIG. 11. (a) Capacitive response energy spectra $R_C(E)$ for $g(E)$ of Fig. 6 as a function of bias voltage following laser pulse excitation. (b) Corresponding net charge flow energy spectra $R_Q(E)$ for the conditions described in (a).

present with an order-of-magnitude greater concentration. In a voltage pulse experiment one would expect a much greater influence on the current transient signal than capacitance due to the greater surface sensitivity for currents due to majority-carrier emission. This is exactly the effect exhibited in Figs. 12(a) and 12(b). Note also the different variations between the bulk and "surface" trap signals with voltage pulse amplitude. The surface signal appears abruptly for both capacitance and current as soon as the surface potential during filling is less than the trap depth. The bulk trap signals, on the other hand, increase monotonically with the voltage pulse amplitude and saturate. This behavior is quite general and may be used to distinguish near surface states from bulk levels.

As a final illustration of our techniques, we use Eqs. (32) and (33) to generate "experimental" DLTS spectra for one value of applied bias from the capacitance and charge-transport response energy spectra shown in Figs. 10 and 11. The resulting spectra are shown in Figs. 13(a) and 13(b). The boxcar gate settings indicated in the figure caption correspond to a time constant τ_m of 100 ms. Apart from the overall sign difference (which reflects the order of subtraction in the DLTS algorithm), these spectra differ from their counterpart response energy spectra in two major respects. First, there is a temperature weighting factor [see Eq. (31)] that changes the relative peak heights. Second, whereas the temperature positions of the *capacitance* DLTS peaks are given by $T_n = E_n / k \ln(\nu\tau_m)$ as expected, the current DLTS peaks occur at a slightly higher temperature. This behavior is well known; it occurs because current transients involve one extra time derivative.

To be accurate we should also point out that our approximation does not strictly apply for the spectra shown in Figs. 13(a) and 13(b) since for the deepest trap $kT_n \simeq 30$ meV which is comparable to

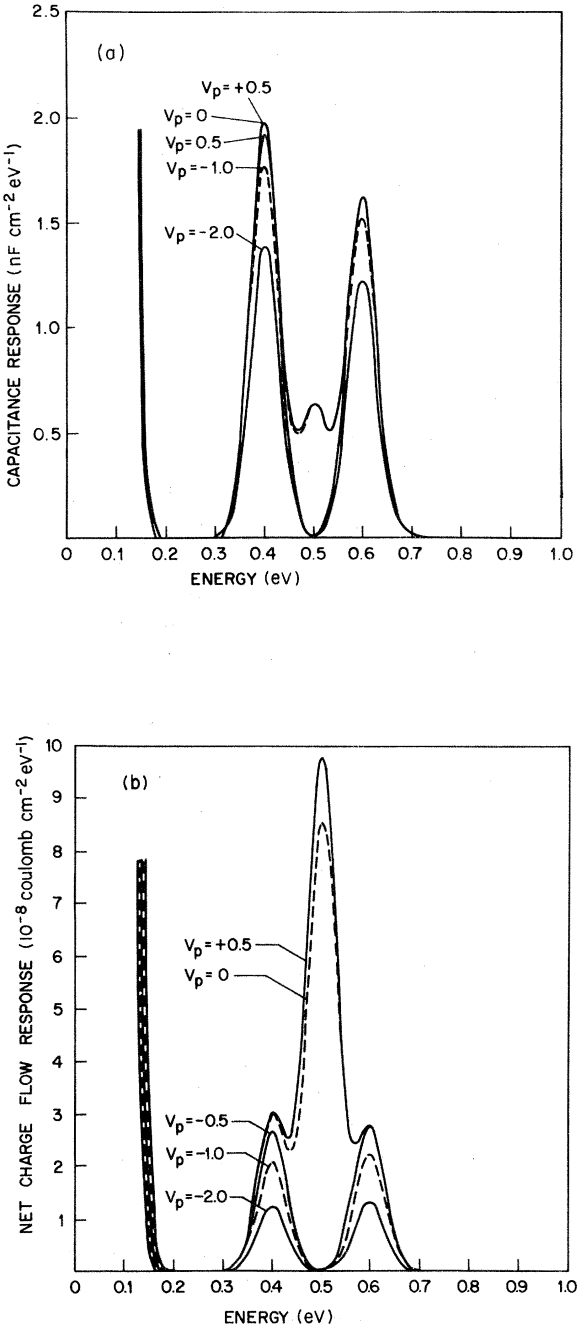

FIG. 12. (a) Capacitive response energy spectra $R_C(E)$ for a sample which has a "surface" region of 500 Å containing a single trap level 0.5 eV below E_c of total integrated concentration 1×10^{16} cm^{-3}. Beyond this 500-Å region, $g(E)$ is given by Fig. 6. Note the variation of the surface trap signal with filling pulse amplitude and the relatively low sensitivity to this level compared with the two bulk levels. (b) Net charge flow energy spectra $R_Q(E)$ for conditions described in (a). Note, in this case, the large sensitivity to the surface trap level.

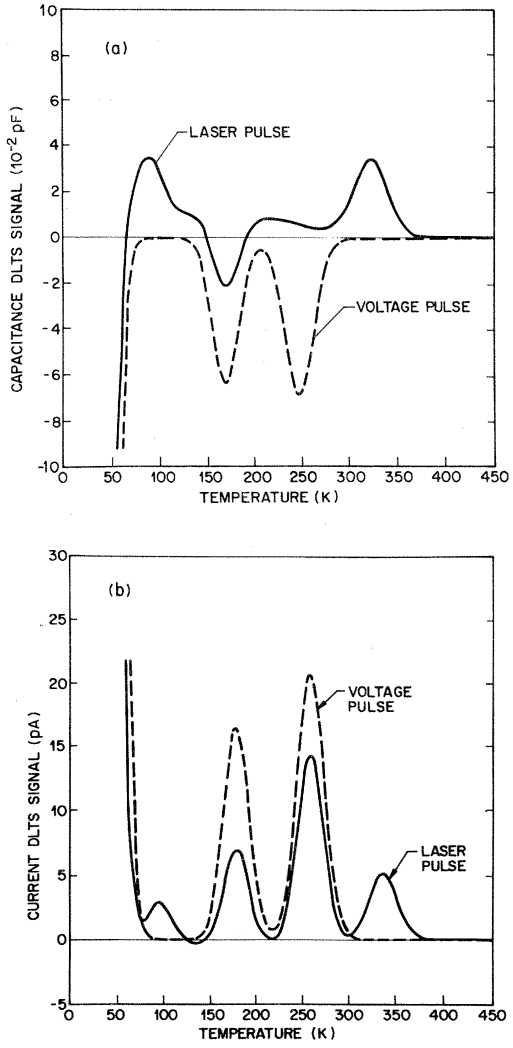

FIG. 13. (a) Capacitance DLTS spectra for a 10-s^{-1} rate window. These spectra were calculated from the 5-V reverse bias response spectra $R_C(E)$ shown in Figs. 10(a) and 11(a) using Eq. (32) with $t_1=50$ ms, $t_2=175$ ms, and $\Delta t=30$ ms, and a junction area A of 2×10^{-3} cm^2. (b) Current DLTS spectra for a 10-s^{-1} rate window. These spectra were calculated from the 5-V reverse bias response spectra $R_Q(E)$ shown in Figs. 10(b) and 11(b) using Eq. (33) with $t_1=50$ ms, $t_2=175$ ms, and $\Delta t=30$ ms, and a junction area of 2×10^{-3} cm^2.

the width of these Gaussian levels. In this particular example, restricting temperatures to, say, less than 100 K, would ensure the accuracy of our methods. However, the remainder of this paper will deal with examples of $g(E)$ where temperatures exceeding even 500 K will pose no such problems.

B. Constant density of states

We next consider a relatively straightforward continuous density of states, that of $g(E)=\text{const}\equiv g$. This density of states is shown in Fig. 14. For small values of applied bias the band bending is given by the well-known exponential function,

$$\psi(x)=V_S\exp(-x/x_0)\ ,$$

where

$$x_0=(\epsilon/qg)^{1/2}\ . \tag{43}$$

For larger values of bias there are two regions—an exponential tail region and a parabolic deep depletion region (see Fig. 2).

The exponential approach to neutral material in the bulk precludes any well-defined meaning of a "depletion width." Figure 15 shows that, indeed, the admittance varies quite markedly with temperature. Artificial truncation of $\psi(x)$ at some arbitrary value (say $2kT$) to define a "width" as discussed by some workers[12] does *not* give the correct value for capacitance. Operationally, a depletion width is a useful concept only to the degree that capacitance is independent of temperature (or frequency).

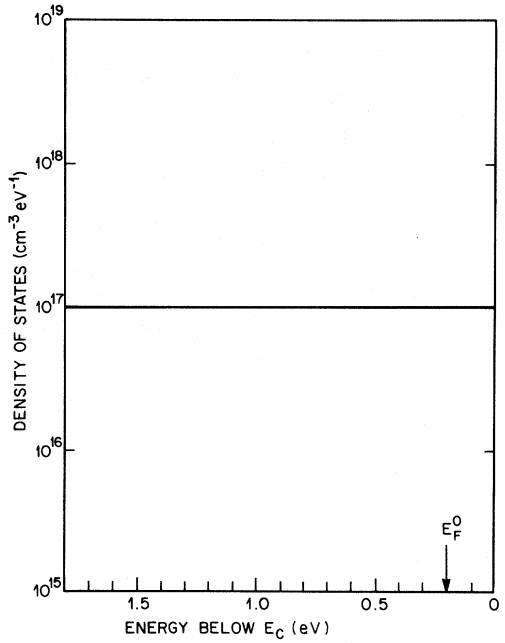

FIG. 14. Density of states for $g(E)=\text{const}=10^{17}$ $\text{cm}^{-3}\text{eV}^{-1}$ showing position of bulk Fermi energy and assumed band gap of 1.8 eV.

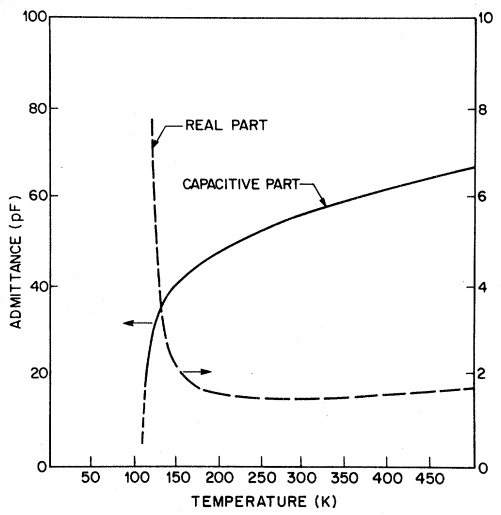

FIG. 15. Imaginary and real part of 10-kHz admittance obtained for density of states of Fig. 14 under 5-V reverse bias ($\phi_B=0.7$ eV). The real part G/ω is expressed in picofarads (pF) and is multiplied by a factor of 10. Note the substantial variation of capacitance with temperature implying the lack of a well-defined depletion width. The junction area A is 2×10^{-3} cm^2.

The capacitive response energy spectrum shown in Fig. 16 further illustrates the kinds of difficulties one can encounter. Neither the overall shape nor quantitative estimates of $g(E)$ using standard formulas enable one to guess the actual density of states. Note, however, that the *trend* for the signal to decrease with energy does agree with the behavior shown for the quasidiscrete spectra. One way of attempting at least an order-of-magnitude estimate for $g(E)$ is via Eq. (36). At a given temperature T the experimental DLTS spectrum, via Eq. (31), gives the capacitance change per unit energy at $E_T=kT\ln\nu\langle t\rangle$. If, for C_0, we use the value of the steady-state capacitance, $C(T)$, and for N_S, the value indicated by the variation of C with bias voltage using the standard profiler formula,[30]

$$N_{CV}(T)=-\frac{C^3(T)}{\epsilon qA^2}\left[\frac{dC(T)}{dV_B}\right]^{-1}\ . \tag{44}$$

Equation (36) then gives an estimate for $g(E_T)$ from the variation of $R_C(E_T)$ with V_p (at small V_p-V_B). However, this serves as an order-of-magnitude estimate only as is apparent from Table II. Note that better agreement is obtained, at higher values of V_B and at higher temperatures (energies). This is expected from the discussion of the discrete level case. The level of agreement, of

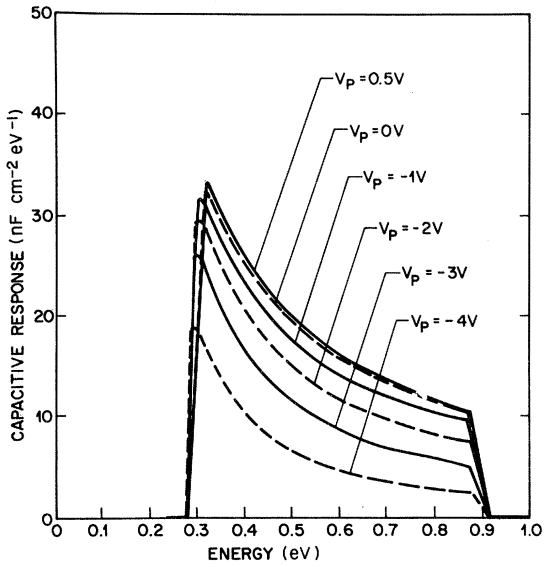

FIG. 16. Capacitive response energy spectra $R_C(E)$ for $g(E)$ of Fig. 14 under -5-V bias as a function of filling pulse voltage. The value V_p refers to the voltage present during filling. The value of the parameter γ, defined by Eq. (35), is 0.7.

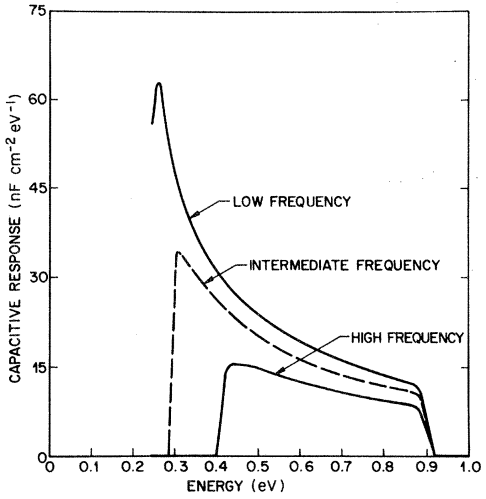

FIG. 17. Capacitive response energy spectra $R_C(E)$ for three values of γ as defined by Eq. (35). The curves for low, intermediate, and high frequency correspond to $\gamma=0.9$, 0.7, and 0.5, respectively. Here $V_B=-5$ V, and $V_p=+0.5$ V is the flat-band voltage.

course, also depends on the particular $g(E)$ involved. These remarks clearly demonstrate the need of detailed analysis to properly interpret DLTS spectra for continuous densities of states.

To obtain Fig. 16 we used a valued of γ [see Eq. (35)] of 0.7 which is appropriate for a 10-kHz measuring frequency with a 100-ms rate window (or a 1-MHz measuring frequency with a 1-ms rate window, etc.). The effect of changing γ is shown in Fig. 17. For a 100-ms rate window the three curves using $\gamma=0.9$, 0.7, and 0.5 correspond to measuring frequencies of approximately 100 Hz, 10 kHz, and 10 MHz. The two most noticeable effects are a shift in the low-temperature cutoff energy and change in the overall magnitude of the signal at higher temperatures. The cutoff arises from the low-temperature freeze-out of the ac response which necessarily shifts to higher temperatures (or energies) as ω is raised. This effect would also be seen for the quasidiscrete $g(E)$ described in the previous section at much lower temperatures. The second effect is due to the frequency-dependent capacitance caused by the response of deep traps to the ac voltage. This effect would not be seen in

TABLE II. Method of estimating the gap state concentration for a material with a continuous density of states. This method uses the standard profiler formula [Eq. (44)] to compute N_{CV} at each temperature and the variation of the DLTS signal with filling pulse [Eq. (36)] to obtain an estimate for $g(E)$ as described in the text. For this example, the "sample" has a *constant* density of states of 1.00×10^{17} cm^{-3}eV^{-1} which is to be compared with the estimated values shown at the extreme right. Note that such an approximate analysis gives at best order-of-magnitude agreement to the actual $g(E)$.

Energy depth (eV)	T_E for 10-s^{-1} rate window (K)	10-kHz capacitance at T_E (pF)	$N_{CV}(T_e)$ (10^{16} cm^{-3})	$\partial\Delta C/\partial V_p$ (pF/V)	Estimated $g(E)$ (10^{17} cm^{-3}eV^{-1})
0.3	123.5	31.8	3.32	36.1	8.18
0.4	164.4	42.9	4.47	21.2	3.57
0.5	205.8	47.9	5.00	13.9	2.10
0.6	247.0	51.6	5.38	10.0	1.40
0.7	288.2	54.6	5.69	7.8	1.03
0.8	329.3	57.2	5.96	6.5	0.82
0.9	370.5	59.4	6.21	5.4	0.65

the quasidiscrete example provided $N_S >> N_T$. Figure 17 suggests an inherent advantage for low-frequency measurements. In practice one must balance this against the better signal-to-noise ratio and higher device Q's obtained at higher frequencies.

In Figs. 18(a) and 18(b) the variation of capacitance and charge transport is shown as a function of bias voltage. Here V_p is the flat band voltage for all cases. As with the quasidiscrete spectrum, the variation of the capacitance signal with V_B is quite complicated. Notice that at low energies the signal varies inversely with V_B, whereas for higher-energy emission nearly the opposite dependence is exhibited. Also note that the capacitance spectrum tends to flatten out (to better mimic the actually density of states) at larger bias, whereas for charge transport [Fig. 18(b)] the signal increases more or less monotonically with V_B. In both regards this behavior is similar to the quasidiscrete case.

Figures 19(a) and 19(b) show the corresponding laser pulse spectra. From our earlier discussion one expects to see the sum and difference of the upper and lower halves of the gap for charge transport and capacitance, respectively. Thus for capa-

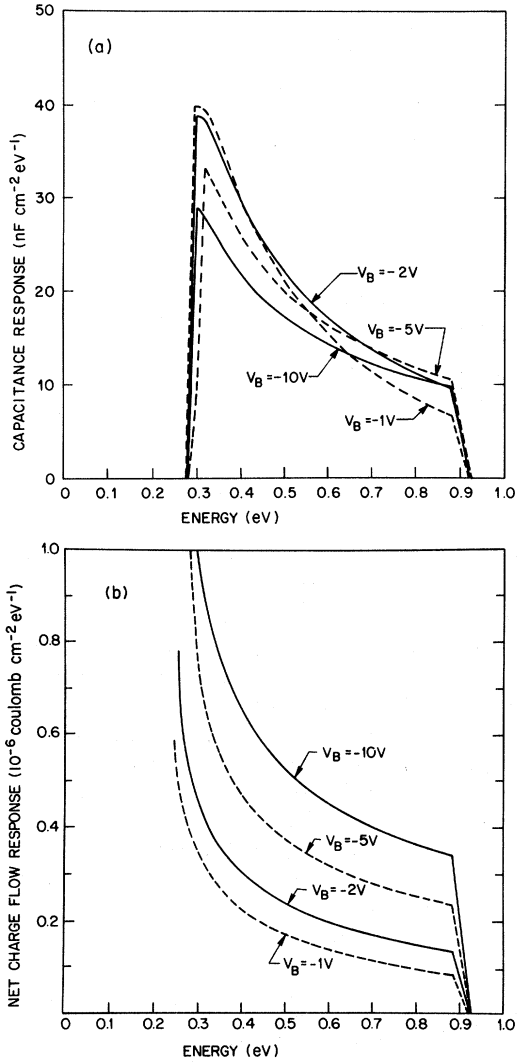

FIG. 18. (a) Capacitive response energy spectra $R_C(E)$, for $g(E)$ of Fig. 14 as a function of bias voltage. In each case the filling pulse voltage V_p is the flat-band voltage. The value of γ is 0.7. (b) Corresponding net charge flow energy spectra $R_Q(E)$ for the conditions described in (a).

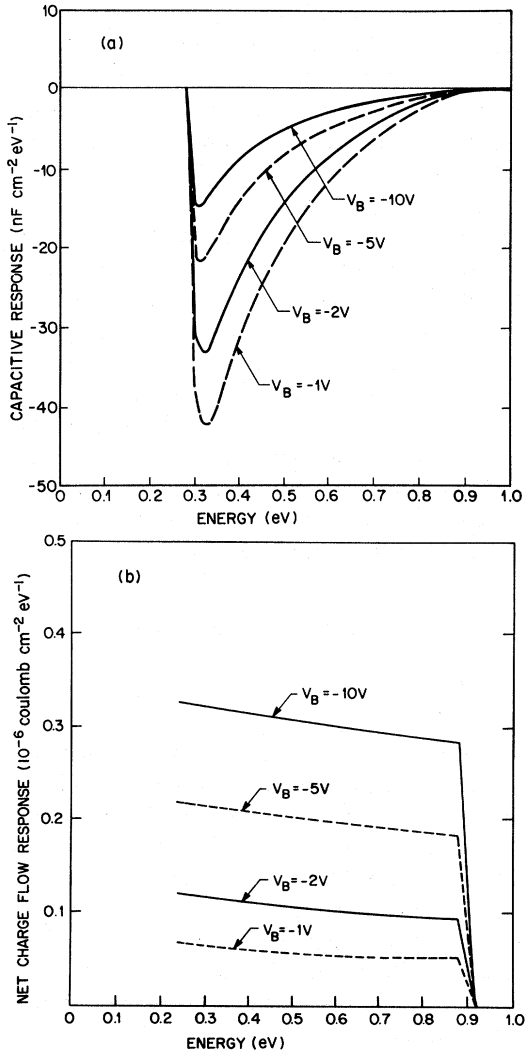

FIG. 19. (a) Capacitive response energy spectra $R_C(E)$ of Fig. 14 as a function of bias voltage following laser pulse excitation. The value of γ is 0.7. (b) Corresponding net charge flow energy spectra $R_Q(E)$ for the conditions described in (a).

citance, one expects to see little or no signal. Instead, a predominantly holelike signal is observed which decreases with increasing V_B. Recalling the negative baseline for the quasidiscrete case, we immediately associate this with electron capture into the tail region of the space-charge region. The charge-transport signal, on the other hand, is surprisingly constant. This is due to the adding of two signals (from the electron and hole emission) whose spatial sensitivities vary in a roughly complementary manner.

Finally, as shown in Figs. 20(a) and 20(b), we again construct actual temperature-scan DLTS spectra from Eqs. (32) and (33) for one value of bias and a 100-ms rate window. The predominant change to the shape of these spectra as compared to Figs. 18 and 19 comes from the kT temperature factor. Note that now the voltage pulse capacitance spectrum has a striking resemblance to the true $g(E)$. This is a quite common occurrence for continuous densities of states. One would normally expect that by dividing the DLTS spectrum by temperature a better representation for $g(E)$ would be obtained. However, for continuous densities of states where comparable numbers of shallow and deep levels are present, the nonlinearity in the capacitance response is such that the signal due to the charge emitted from a fixed energy increment tends to *decrease* with increasing temperature [see Fig. 18(a)]. Thus the raw DLTS spectrum often provides a better representation of $g(E)$. This point should be kept in mind as we turn to consider the additional examples below.

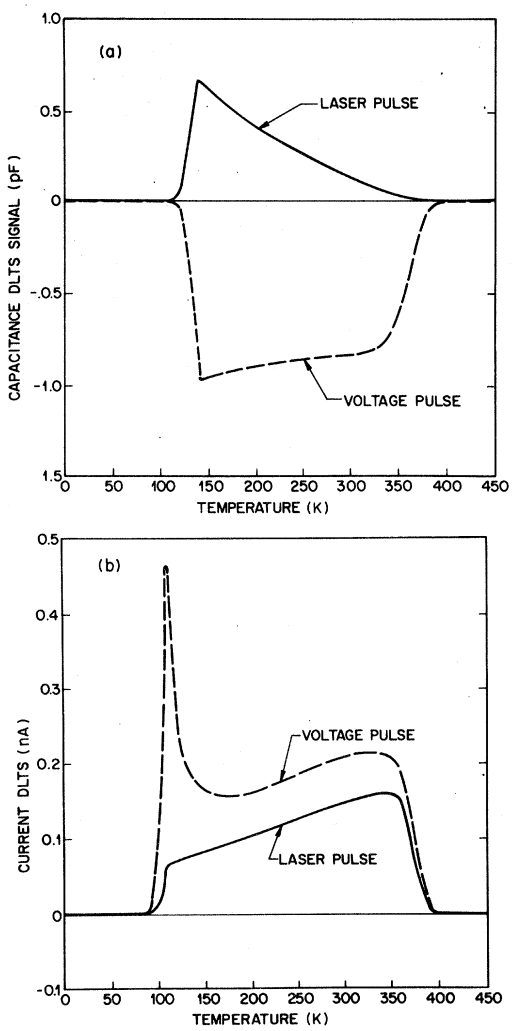

FIG. 20. (a) 10-kHz capacitance DLTS spectra for a 10-s^{-1} rate window. These spectra were calculated from the 5-V reverse bias response spectra $R_C(E)$ shown in Figs. 18(a) and 19(a) using Eq. (32) with $t_1=50$ ms, $t_2=175$ mS, and $\Delta t=30$ ms. Note the resemblance of the voltage pulse DLTS spectrum to the actual density of states. The junction area A is 2×10^{-3} cm^2. (b) Current DLTS spectra for a 10-s^{-1} rate window. These spectra were calculated for the 5-V reverse bias response spectra $R_Q(E)$ shown in Figs. 18(b) and 19(b) using Eq. (33) with $t_1=50$ ms, $t_2=175$ ms, and $\Delta t=30$ ms, and a junction area of 2×10^{-3} cm^2.

C. Additional case studies

We now consider a host of examples of possible relevance for the study of semiconductors with large continuous distributions of deep gap states. Most of the densities of states to be considered are similar to some being proposed for amorphous semiconductors. For each $g(E)$, we will specifically calculate the expected result for 10-kHz admittance versus temperature under reverse bias and both the 10-kHz capacitance and current DLTS spectra (at a 100-ms rate window) for reasonably highly doped material ($\Delta E_F=0.2$ eV) with a junction area of 2×10^{-3} cm^2. Toward the end of this section we will compare the above results with C-V measurements for each case and finally consider one alternate approach for materials that are more highly insulating (large ΔE_F).

To treat a larger number of possible cases we recall that admittance and voltage pulse DLTS depend, under our assumptions, only on $g(E)$ above midgap. Therefore, in each of Figs. 21–23 we match one $g(E)$ for the upper-half gap with three possibilities for the lower-half gap, thereby encompassing, with the inclusion of Fig. 24, ten possible densities of states. We also point out that these examples are extended trivially to multiplication of

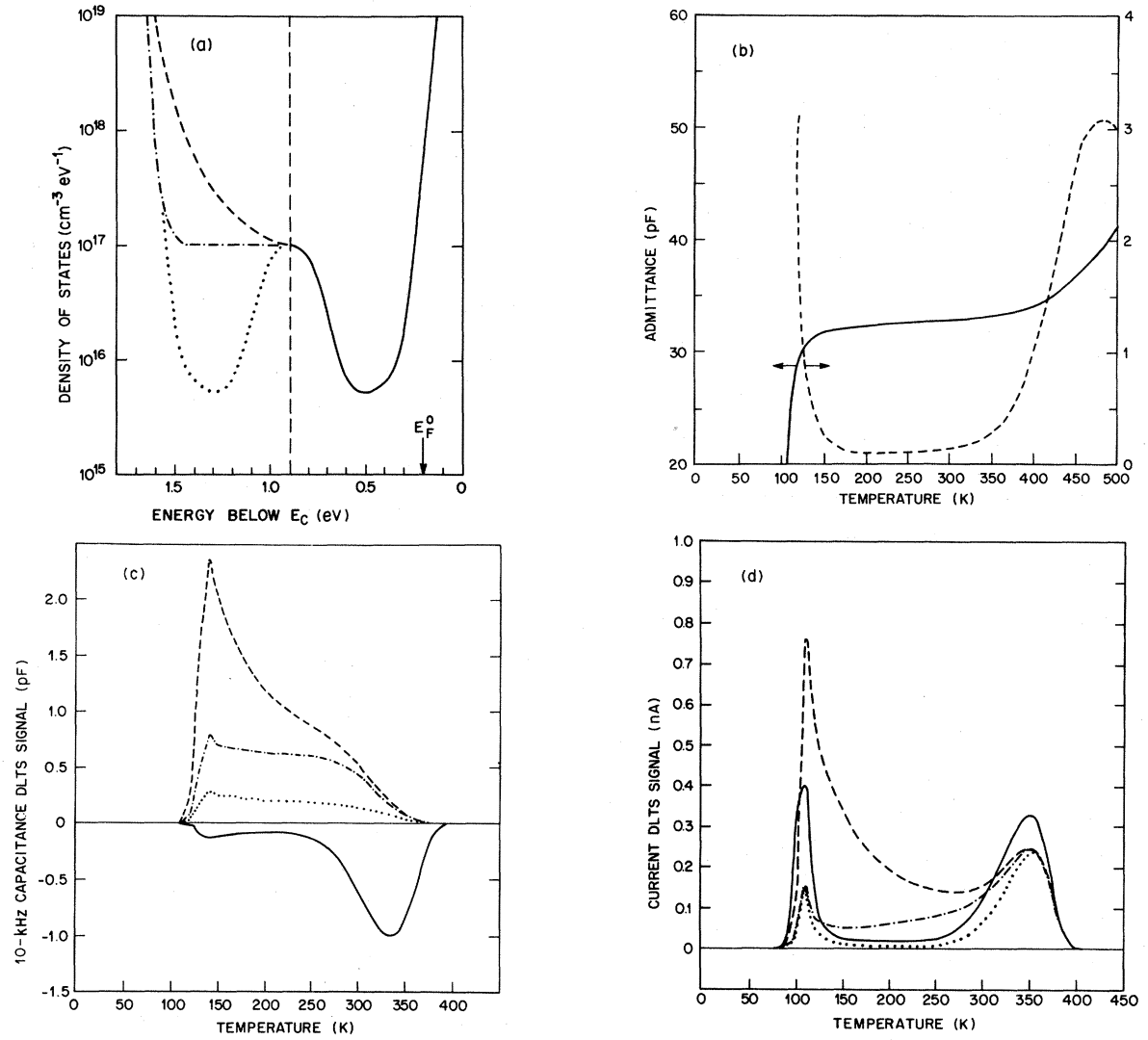

FIG. 21. (a) Center-peaked density of states (dotted line) with two variations below midgap indicated by the dashed and dashed-dotted lines. (b) Capacitive (solid line) and real part G/ω (dashed line) of 10-kHz admittance for $g(E)$ of (a) with $V_B=-5$ V. (c) 10-kHz capacitance DLTS for a 10-s^{-1} rate window for $g(E)$ of (a) with $V_B=-5$ V. The laser pulse spectrum depends on features of $g(E)$ below midgap as indicated. (d) Current DLTS for a 10-s^{-1} rate window for $g(E)$ of (a) with $V_B=-5$ V. The laser pulse spectrum depends on features of $g(E)$ below midgap as indicated. *Notes for Figs. 21—23:* In each (a) part, three densities of states are displayed which overlap in the upper half of the gap ($E_g=1.8$ eV). In each (b) part the resulting 10-kHz admittance vs temperature is shown at 5-V reverse bias which is identical, under our assumptions for all three cases shown in (a). In each (c) and (d) part, 10-kHz capacitance and current DLTS spectra are displayed. The solid line represents voltage pulse filling which is determined wholly by the common features of $g(E)$ in the upper half of the gap. The dotted, dashed, and dashed-dotted lines for laser pulse excitation are calculated from the corresponding continuation of $g(E)$ into the lower half of the gap as shown in (a). In all cases $V_B=-5$ V and V_p is the flat-band voltage ($+0.5$ V). The junction area is 2×10^{-3} cm^2.

$g(E)$ by any constant factor due to the scaling properties of Poisson's equation. That is, multiplication of $g(E)$ by the constant factor F merely increases all capacitance and current values by $F^{1/2}$, while leaving the temperature and energy dependences unchanged.

Let us now consider each of Figs. 21—24 in slightly more detail. Figure 21 includes the cases of a broad peak in $g(E)$ near midgap as well as one proposed density of states for n-type a-

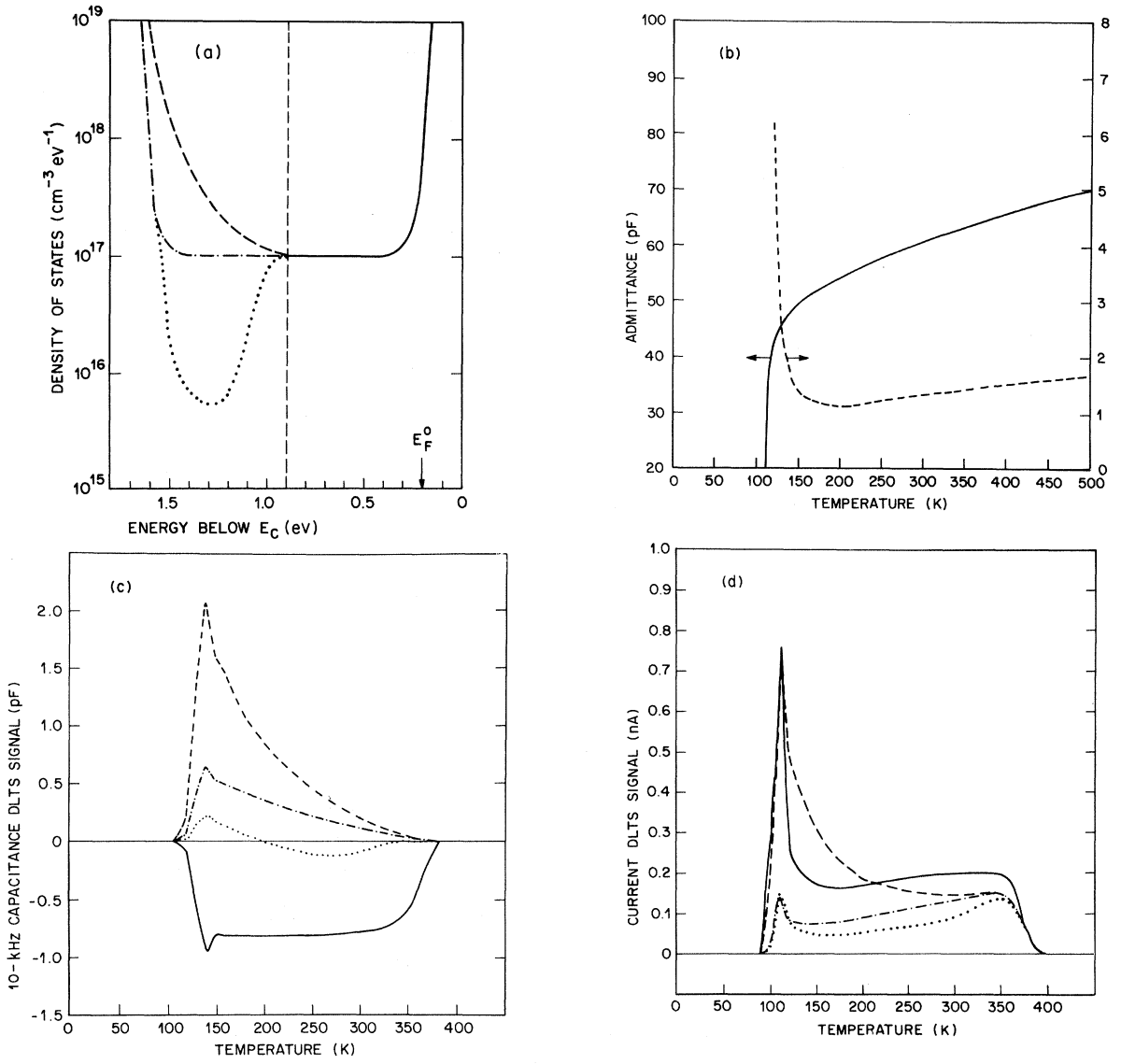

FIG. 22. (a) Flat density of states (dashed-dotted line) with two variations below midgap indicated by the dashed and dotted lines. (b) Capacitive (solid line) and real part G/ω (dashed line) of 10-kHz admittance for $g(E)$ of (a) with $V_B = -5$ V. (c) 10-kHz capacitance DLTS for a 10-s^{-1} rate window for $g(E)$ of (a) with $V_B = -5$ V. The laser pulse spectrum depends on features of $g(E)$ below midgap as indicated. (d) Current DLTS for a 10-s^{-1} rate window for $g(E)$ of (a) with $V_B = -5$ V. The laser pulse spectrum depends on features of $g(E)$ below midgap as indicated.

Si:H,[10,20] with and without a large hole tail. The admittance [Fig. 21(b)] shows a broad plateau whose value is determined roughly by the total integrated number of gap states between the Fermi energy and midgap. In capacitance DLTS [Fig. 21(c)], we see a prominent peak at high temperatures for voltage pulse filling and a broad band of hole states under laser excitation. Except for the symmetric case, the spectral shape mimics qualitatively the actual $g(E)$.

Figure 22 includes a case very similar to that of Sec. II B [constant $g(E)$], except the shallow-state density is increased due to the band tailing. This produces slight changes in both admittance and DLTS. This figure also includes the reverse of one case in Fig. 21 which might be relevant for p-type a-Si:H. Note that for this subcase, the predominance of states in the upper half of the gap actual-

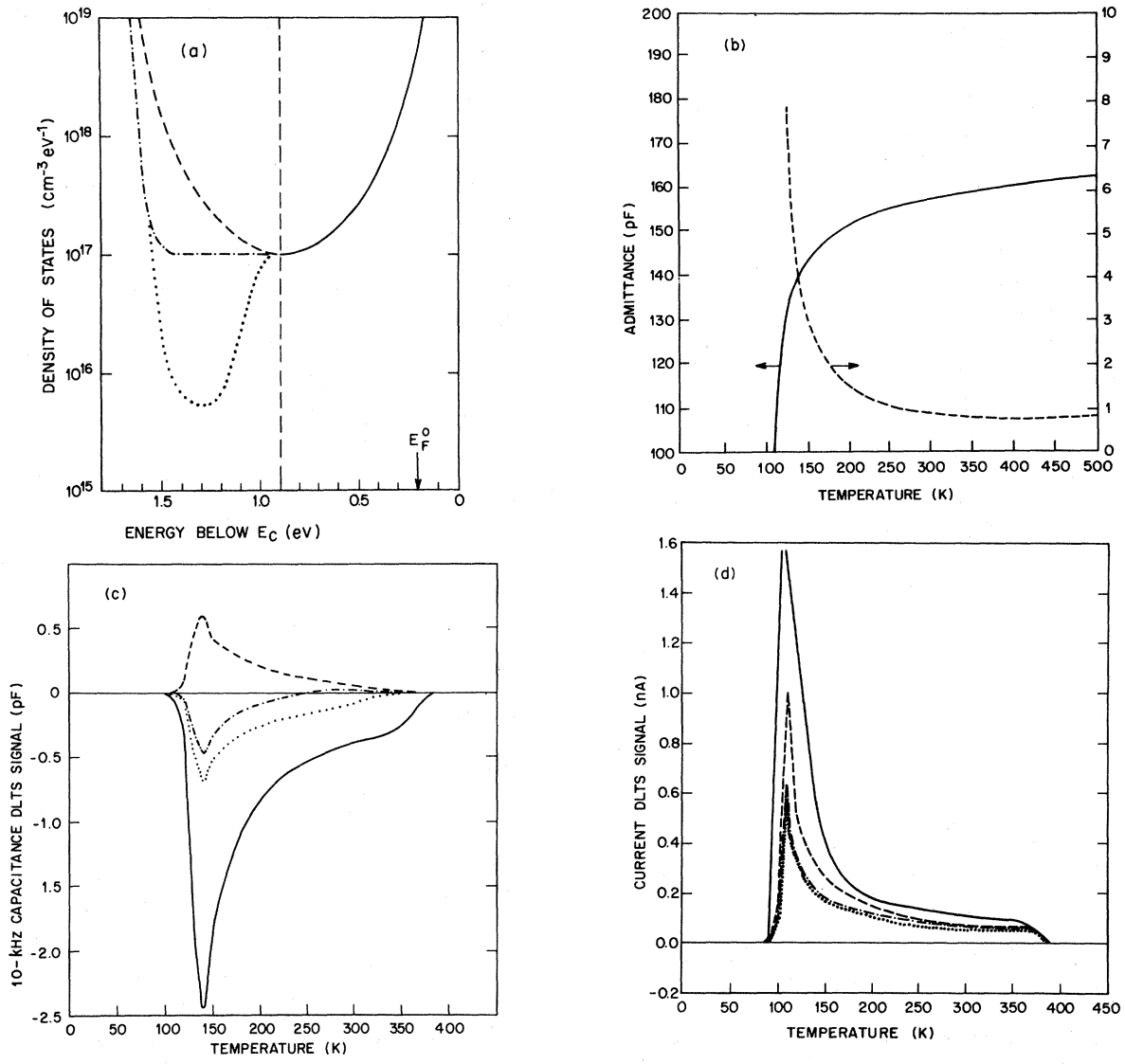

FIG. 23. (a) *U*-shaped density of states (dashed line) with two variations below midgap indicated by the dashed-dotted and dotted lines. (b) Capacitive (solid line) and real part G/ω (dashed line) of 10-kHz admittance for $g(E)$ of (a) with $V_B=-5$ V. (c) 10-kHz capacitance DLTS for a 10-s^{-1} rate window for $g(E)$ of (a) with $V_B=-5$ V. The laser pulse spectrum depends on features of $g(E)$ below midgap as indicated.

ly give rise to a *negative* laser pulse capacitance DLTS signal. This is expected since laser-induced capacitance transients reflect the *difference* between electron and hole emission. Indeed, it is perhaps unexpected that the negative signal level should be so small.

Figure 23 includes a case similar to one density of states obtained from *C-V* analysis for *a*-Si:H.[11] It also includes *p*-type analogs of two cases shown in Figs. 21 and 22. Note that the admittance curve [Fig. 23(b)] is qualitatively similar to Fig. 22(b) (although with greater curvature at higher temperature). Thus, while distinguishing the densities of states of Figs. 22(a) and 23(a) might be difficult on the basis of admittance, the DLTS signal is markedly different and again gives a good qualitative picture of $g(E)$. In this case, as with Fig. 22, we again see examples of an electronlike laser-induced DLTS signal.

Finally, in Fig. 24(a), we consider the well-

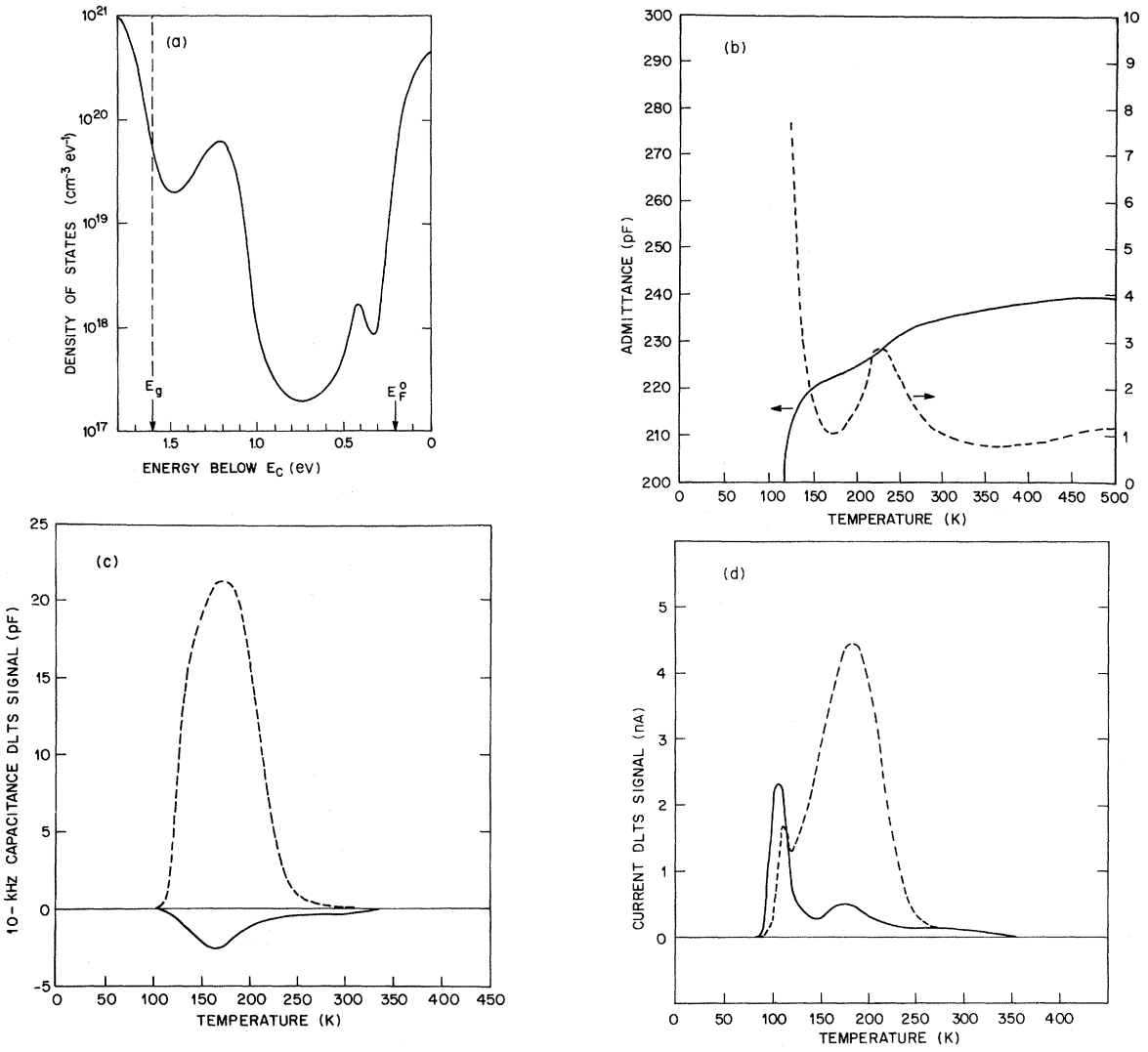

FIG. 24. (a) Density of states as determined for a-Si:H from field-effects measurements of Spear and co-workers (Refs. 31 and 32). Note that $E_g = 1.6$ eV. (b) Capacitive (solid line) and real part G/ω (dashed line) of 10-kHz admittance for "Spear" $g(E)$ with $V_B = -5$ V. (c) 10-kHz capacitance DLTS for a 10-s^{-1} rate window for Spear $g(E)$ with $V_B = -5$ V. The solid line is the voltage pulse spectrum with $V_p = +0.5$ V (the assumed flat-band voltage). The dashed line is the laser pulse spectrum. (d) Current DLTS for a 10-s^{-1} rate window for Spear $g(E)$ with $V_B = -5$ V. The solid line is the voltage pulse spectrum and the dashed line is the laser pulse spectrum.

known density of states obtained for a-Si:H from field-effect measurements.[31,32] The sharp peak in the upper half of the gap (at 0.4 eV) is easily observable in admittance [Fig. 24(b)] and voltage pulse DLTS [Figs. 24c and 24(d)]. The very large peak in the lower-half gap shows up prominently in laser pulse DLTS.

One thing that should be clear from these examples is the relative advantage of DLTS over admittance to deduce the underlying density of states. The qualitative similarity between the measured DLTS signals and $g(E)$ is an enormous advantage when attempting a detailed analysis of actual measurements (see Ref. 10). However, admittance versus T measurements are also generally useful, are relatively easy to perform and often disclose prominent features in $g(E)$. This is to be contrasted with C-V measurements where vastly different densities of states produce only subtle changes. In Fig. 25 we plot the results of C-V measurements, calculated for 10 kHz at room temperature, for each of the cases shown in Figs. 21—24. Since the

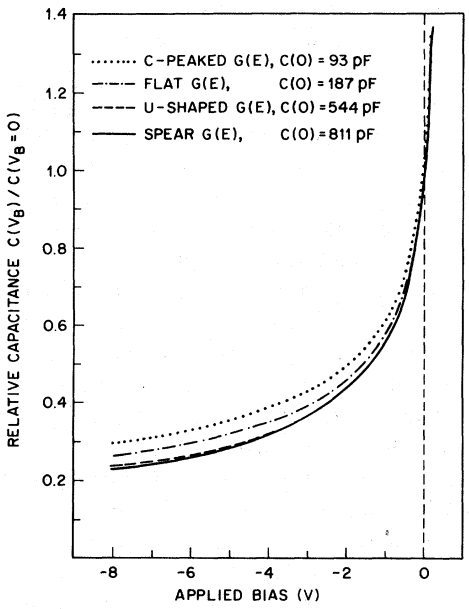

FIG. 25. 10-kHz capacitance vs applied voltage at room temperature for a Schottky-barrier diode with four different densities of states. The dotted, dashed-dotted, dashed, and solid lines correspond to Figs. 21–24, respectively. These C-V curves have been rescaled to have the same value at zero applied volts (the flat-band voltage is +0.5 V) with the actual value of zero-voltage capacitance noted in the diagram. Note the close similarity of all four curves, particularly of those orginating from Figs. 23 and 24.

scale factor is related only to the overall magnitude of $g(E)$, we have plotted these curves to overlap at $V_B=0$ and have indicated the value of $C(0)$ for each case in the diagram.

It would be difficult (at best) to obtain $g(E)$ very accurately from such C-V data. The most accessible information contained in such curves is an estimate of the total number of states (between E_F^0 and midgap) obtained through Eq. (44).

For highly insulating material, for which ΔE_F is greater than 0.6 eV, such methods as low-frequency C-V are perhaps not so easily dismissed. Certainly DLTS becomes almost impossible to perform under such conditions. The recent approach of several workers to employ admittance versus temperature measurements for these materials[14,15] is perhaps the best alternative, in particular because measurements of this kind made under different applied bias could be used to test for spatially inhomogeneous films. Along these lines we will consider one possible approach using admittance versus temperature measurements to deduce the magnitude and, in some cases, the slope of $g(E)$ just below E_F^0.

In Fig. 26(a) the 10-kHz admittance for each $g(E)$ shown in Figs. 21–23 is compared for a case where the Fermi energy E_F^0 is now assumed to lie 0.6 eV below E_c. Since the magnitude of $g(E)$ is comparable in these three cases near midgap, the capacitance for each case is also comparable and varies roughly with the total integrated number of states between E_F^0 and $Eg/2$. The magnitude and slope of $g(E)$ below E_F^0 is related to the slope and curvature of these admittance curves; however, the correlation is certainly not obvious. Moreover, possible anomalies near the surface of real films[22–24] would be particularly troublesome if such a detailed analysis were attempted on a raw admittance data.

The interpretation becomes somewhat more straightforward if the temperature dependence of the quantity $C^2(dC/dT)^{-1}$ is considered. From the expression derived for admittance in Sec. II C [Eq. (27)], one can readily demonstrate that this quantity will be *independent* of applied bias *provided* the film is spatially uniform over the region where the ac charge distribution is nonzero (beyond the point x_1 as defined in Sec. II C). Furthermore, if we expand $g(E)$ in a Taylor series around the neutral bulk Fermi energy E_F^0,

$$g(E)=g_0(E_F^0-E)+g_1\frac{(E_F^0-E)^2}{2}+\cdots, \tag{45}$$

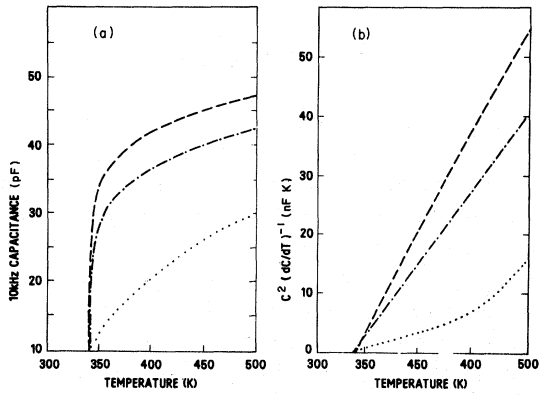

FIG. 26. In (a) 10-kHz capacitance vs temperature displayed for the three densities of states shown in Figs. 21(a)–23(a) (as indicated by the dotted, dashed-dotted, and dashed lines, respectively), where now the bulk Fermi level E_F^0 is assumed to lie 0.6 eV below E_c. (b) Ratio $C^2(dC/dT)^{-1}$ is plotted vs temperature. As explained in the text, the slope and curvature of these curves are directly related to the value and slope, respectively, of $g(E)$ at E_F^0.

then it also follows from Eq. (27) that

$$C^2(T)\left[\frac{dC}{dT}\right]^{-1} = A(\epsilon q g_0)^{1/2}\left[(T-T_0) + \frac{1}{3}\frac{g_1}{g_0}(T-T_0)^2 \times k\ln\left[\frac{\nu}{\omega}\right] + \cdots\right], \tag{46}$$

where T_0 is the "freeze-out" temperature of the ac response (approximately 340 K in Fig. 26). Thus, the first and second derivatives of $C^2(T) \times (dC/dT)^{-1}$ are directly related to the magnitude and slope of $g(E)$ at E_F^0.

In Fig. 26(b) this behavior is illustrated. The density of states in Fig. 21, which has a relatively low value and a positive slope at $\Delta E_F = 0.6$ eV, shows a relatively small slope and positive curvature for $C^2(T)(dC/dT)^{-1}$. On the other hand, the density of states in Fig. 23, which is larger but slightly decreasing at $\Delta E_F = 0.6$ eV, shows a larger slope and slight negative curvature. Care should be taken, as with all admittance measurements, to apply this analysis to temperatures sufficiently above the "turn-on" of the ac response. The somewhat high temperatures indicated in Fig. 26 can, of course, be reduced by lowering the measuring frequency. An application of this kind of analysis to experimental data can be found in Ref. 10.

IV. DISCUSSION

In this paper we have demonstrated a method of solution for the thermally stimulated transient response of a Schottky-barrier space-charge region for a semiconductor with a continuous density of states. The method is quite general and applies to any material with an arbitrarily shaped $g(E)$ with or without spatial variation. We have adopted various assumptions, listed at the beginning of Sec. III, of which some are necessary for our method of analysis with several others adopted for calculational convenience or because they are believed pertinent to actual materials. In this setting we examined several specific cases of interest including one of nearly discrete levels, to make contact with crystalline work, and several which are potentially relevant to the study of amorphous semiconductors. These cases were treated primarily within the context of two relatively versatile measurement techniques: admittance versus temperature and DLTS.

Our methods of analysis help fill a long standing need of extending electrical transient measurements from the very successful studies of gap states in crystalline semiconductors to new classes of semiconducting materials with large concentrations of gap states for which the basic principles of capture and emission from these states or even transport itself may not be well understood. Only through a detailed understanding of the basic junction response, which allows direct comparison among a variety of measurements, will unusual and perhaps basic new behavior of such materials be recognized and investigated. For example, whereas a capacitance DLTS spectrum may be calculated, under our assumptions, for practially any given density of states the converse is *not* true: we cannot generate certain classes of DLTS spectra no matter how we change the density of states. Were such spectra to be observed, some of our assumptions would have to be changed. By requiring that a given density of states also agree with current DLTS, admittance, TSCAP, *C-V* and other measurements, the sets of possible assumptions become very limited indeed.

In Ref. 10 these calculational methods are applied to a detailed investigation of the properties of *a*-Si:H. In some cases a simpler analysis had indicated possible discrepancies between admittance, TSCAP, and DLTS. The fact that these can now be resolved speaks quite strongly for the general validity our assumptions for that material. Nonetheless, certain inconsistencies remain between this work and some of the work of other researchers. Through our method of analysis these inconsistencies may now be linked rather convincingly to surface and near-surface anomalies in these films.

In this regard it is important to reemphasize those techniques which have been demonstrated to be least susceptible to near-surface spatial anomalies. As discussed in Sec. III, these are notably capacitance DLTS, particularly when performed at large reverse bias and relatively small filling pulse voltages and, to some degree, admittance versus temperature, also when performed at larger values of reverse bias. For the latter measurement, the ratio $C^2(T)[dC/dT]^{-1}$ was found to be even less sensitive to regions near the barrier interface and is perhaps the best candidate for obtaining information about $g(E)$ in undoped materi-

als (Fermi energy near midgap).

From such remarks it should also be clear that without the complete methods of analysis of transient behavior at our disposal the signature of truly new physical phenomena could be easily obscured. Ultimately it is hoped that thermal transient measurements on diode junctions may disclose in amorphous semiconductors the existence of negative-U or other complex centers as they already have in crystals.[33,34] Perhaps such measurements may even allow the nature of the mobility edge or hopping conduction to be explored. Since our analysis has been presented in a very general way, it may easily be extended to include fairly complicated trapping behavior or to using other detection schemes for observing different aspects of transient behavior in space-charge regions. Indeed, some of these applications will most probably be discussed at length in the near future.

ACKNOWLEDGMENTS

We wish to acknowledge J. P. Harbison and G. A. Baraff for helpful discussions. We especially thank V. Narayanamurti for enthusiastic interest and encouragement during the course of this work.

APPENDIX A: NOUMEROV ANALYSIS OF SPACE-CHARGE REGION

The Noumerov technique provides a rapidly converging algorithm for numerically solving the integral differential equation describing the band bending in the space charge [Eq. (1)]. For an equation of the form

$$P''=Q\ , \tag{A1}$$

one usually divides the interval of interest into N equal steps of size h and denotes the values of the functions P and Q at the ith point as P_i and Q_i, respectively. In the usual case, Q is a known function and the Noumerov method relates the value of P at the next point, P_{i+1}, to its values at the preceding points:

$$P_{i+1}=2P_i-P_{i-1}+h^2Q_i + \frac{h^2}{12}(Q_{i+1}+Q_{i-1}-2Q_i) + O(h^6P^{(vi)})\ . \tag{A2}$$

As indicated, this method is accurate to *sixth* order in P. The problem, in our case, is that Q is given by an integral which depends on P so that the quantity Q_{i+1} is not known. Specifically,

$$Q=\frac{q}{\epsilon}\int_{-\Delta E_F-P}^{-\Delta E_F} g(E',x)dE'\ . \tag{A3}$$

We define

$$P^*_{i+1}=2P_i-P_{i-1}+h^2Q_i\ , \tag{A4}$$

and note that this is equal to P_{i+1} to fourth order in P. Therefore

$$Q_{i+1}=\frac{q}{\epsilon}\int_{-\Delta E_F-P^*_{i+1}}^{-\Delta E_F} g(E',x_{i+1})dE' + O(h^4P^{(iv)}P'') \tag{A5}$$

and

$$P_{i+1}=2P_i-P_{i-1}+h^2Q_i + \frac{h^2}{12}(Q^*_{i+1}+Q_{i-1}-2Q_{i-1}) + O(h^6P^{(vi)})+O(h^6P^{(iv)}P'')\ , \tag{A6}$$

where Q^*_{i+1} denotes the value of the integral on the rhs of Eq. (A5). Equation (A6) has the same inherent accuracy as the usual Noumerov case [Eq. (A2)]. For example, if $g=$constant so that P is given by an exponential function, $P\sim\exp(x/x_0)$, then the correction term in Eq. (A6) is of order $(h/x_0)^6$. Thus for a step size which is $1/N$ the characteristic length the overall accuracy is $N(1/N)^6=1/N^5$.

Indeed, for the equilibrium problem such rapid convergence is obtained for most $g(E)$. As few as 10 integration steps over the characteristic width x_0 are often sufficient. When applied to the nonequilibrium case, however, this basic accuracy is somewhat diminished because of the different regions within the space-charge region. As a result, P and Q will exhibit singularities in their higher derivatives at the boundaries of these regions. For the voltage pulse case, where Q is nonetheless a continuous function (see Fig. 3), Eq. (A6) has been applied with good results. The case study in Sec. III A (see Table I) gave roughly a 1% accuracy for the DLTS capacitance signal which itself represented only a 0.1% change of the total capacitance. This overall accuracy of 1 part in 10^5 was achieved with 150 integration steps over the depletion width W. This is quite impressive if we further recognize that, for this case study, $g(E)$ is perhaps the *least* suitable to our methods due to its large higher derivatives.

For the laser pulse calculation Q becomes discontinuous (see Fig. 5) and Eq. (A6) is, by itself, unsuitable. For this situation we must apply this equation to each of the two regions of the space-charge region and match boundary conditions. For spatially homogeneous films, however, this is particularly easy; Eq. (A6) is applied to the equilibrium region (region C of Sec. II B) and then, recognizing that region B will be characterized by a constant charge density, the band potential is extrapolated via the appropriate quadratic function to the metal interface.

APPENDIX B: SOLUTION OF THE LOSEE DIFFERENTIAL EQUATION FOR ADMITTANCE

As discussed in Sec. II C, Losee writes the complex admittance per unit area for a Schottky-barrier space-charge region as

$$Y=i\omega\epsilon\left.\frac{H^{1/2}(\psi)}{W(\psi)}\right|_{\psi=V_s}, \tag{B1}$$

where

$$H(\psi)=\frac{2}{\epsilon}\int_0^{\psi}\rho(\psi')d\psi', \tag{B2}$$

and W satisfies the equation

$$\frac{dW}{d\psi}=1+\frac{\rho}{\epsilon H}W-\frac{F}{\epsilon H}W^2. \tag{B3}$$

Here, ρ is the charge density for a given amount of band bending ψ:

$$\rho(\psi)=q\int_{-\Delta E_F-\psi}^{-\Delta E_F}g(E')dE'. \tag{B4}$$

We argued in Sec. II C that, for a continuous density of states $g(E)$, F will be given by

$$F(\psi,\omega)=qg(-\Delta E_F-\psi)(1+i\omega\tau)^{-1}, \tag{B5}$$

where

$$\tau=\frac{1}{\nu}\exp[(\Delta E_F+\psi)/kT], \tag{B6}$$

is the response time of a localized state at energy depth $\Delta E_F+\psi$. Taking $W=U+iV$, we rewrite Eq. (B3) into its component parts

$$\frac{dU}{d\psi}=1+\frac{\rho}{\epsilon H}U-\frac{1}{\epsilon H}\frac{qg}{1+\omega^2\tau^2}[(U^2-V^2)+2\omega\tau UV], \tag{B7}$$

$$\frac{dV}{d\psi}=\frac{\rho}{\epsilon H}V-\frac{1}{\epsilon H}\frac{qg}{1+\omega^2\tau^2}[2UV-\omega\tau(U^2-V^2)]. \tag{B8}$$

First we consider Eq. (B7) in two limiting cases: (1) small ψ, where $\omega\tau<<1$ and $F=qg(-\Delta E_F+\psi)$, and (2) large ψ, where $\omega\tau>>1$ and $F=0$. In case (1) we can immediately verify that

$$U=\frac{\epsilon H}{\rho},\quad V=0, \tag{B9}$$

is the correct solution since it satisfies Eq. (B7) and also the boundary condition that $W\to 0$ as $x\to\infty$ (see Ref. 5). For case (2) we may verify that $U=-xH^{1/2}$ is a solution of the inhomogeneous equation and that $W=KH^{1/2}$ satisfies the homogeneous equation

$$\frac{dU}{d\psi}=\frac{\rho}{\epsilon H}U.$$

Hence the complete solution is

$$U=KH^{1/2}-xH^{1/2}. \tag{B10}$$

Here, $x=x(\psi)$ is the inverse function of $\psi(x)$. We define $x_1=x(\psi_1)$ by

$$\omega\tau=\frac{\omega}{\nu}\exp[(\Delta E_F+\psi_1)/kT]=1.$$

Consider the behavior at low temperatures. This limit is characterized by a nearly abrupt change from case (1) to case (2) at a distance x_1 from the barrier interface. Thus, we require

$$KH^{1/2}(\psi_1)-x_1H^{1/2}(\psi_1)=\frac{\epsilon H(\psi_1)}{\rho(\psi_1)}$$

or

$$K=\frac{\epsilon H^{1/2}(\psi_1)}{\rho(\psi_1)}+x_1\equiv\frac{\epsilon H_1^{1/2}}{\rho_1}+x_1.$$

Therefore,

$$U(\psi=V_s)=\left[\frac{\epsilon H_1^{1/2}}{\rho_1}+x_1\right]H_0^{1/2}, \tag{B11}$$

where $H_0=H(V_S)$. Hence,

$$\frac{C}{A}=\mathrm{Im}\frac{Y}{\omega}=\epsilon\frac{H_0^{1/2}}{U(V_s)}$$

or

$$C=A\epsilon\frac{\rho_1}{\epsilon H_1^{1/2}+x_1\rho_1}. \tag{B12}$$

For low temperatures we also have $V << U$. Therefore for $\omega\tau << 1$, Eq. (B8) becomes

$$\frac{dV}{d\psi} = \frac{\rho}{\epsilon H} V - \frac{2}{\epsilon H} qgUV ,$$

with $U = \epsilon H/\rho$. The general solution is $V = K'(H^{1/2}/\rho^2)$; however, this solution will not vanish for $x \to \infty$ unless $K' = 0$. Hence, $V = 0$ for $\omega\tau << 1$. For $\omega\tau << 1$, $dV/d\psi = \rho V/\epsilon H$, and hence $V = K'' H^{1/2}$. The constant is determined by integrating V over the region where $\omega\tau \sim 1$. Since this region is assumed small at low T we may take $U = \epsilon H_1/\rho_1 \simeq$ const. Then

$$\frac{dV}{d\psi} = \frac{\rho_1}{\epsilon H_1} V + \frac{\epsilon H}{\rho_1^2} qg(\Delta E_F + \psi_1) \frac{\omega\tau}{1+\omega^2\tau^2} . \tag{B13}$$

The validity of Eq. (B13) follows directly from the assumed small variation of $g(E)$ over energy scales of order kT.

Since the first term on the rhs will be negligible for $V << U$ we obtain

$$\Delta V \simeq \frac{\epsilon H_1}{\rho_1^2} qg(-\Delta E_F - \psi_1) \int \frac{\omega\tau}{1+\omega^2\tau^2} d\psi ,$$

where

$$\omega\tau \propto \exp[(E_F + \psi)/kT] ,$$

and varies from a very small to a very large value over the region in question. Hence,

$$\Delta V = \frac{\epsilon H_1}{\rho_1^2} qgkT \int_0^\infty \frac{dx}{1+x^2} = kT \frac{\epsilon H_1}{\rho_1^2} qg(-\Delta E_F - \psi_1) \frac{\pi}{2} . \tag{B14}$$

For large $\omega\tau$, where $V = K'' H^{1/2}$, we therefore obtain

$$K'' = kT \frac{\epsilon H_1^{1/2}}{\rho_1^2} qg(-\Delta E_F - \psi_1) \frac{\pi}{2}$$

and

$$\mathrm{Re}\frac{Y}{\omega} \simeq -\epsilon \frac{VH^{1/2}}{U^2}\bigg|_{V_s} = -kT \frac{\pi}{2} C^2 \frac{H_1^{1/2}}{\rho_1^2} Aqg(-\Delta E_F - \psi_1) . \tag{B15}$$

Although these expressions have been derived for low temperatures, we have determined the error in using Eqs. (B12) and (B15) to be quite small at temperatures of interest. This error may be estimated a variety of ways. A fairly straightforward method is to integrate Eq. (B7) from $\psi = 0$ to the value ψ_1, where $\omega\tau = 1$. Over this region we neglect the terms containing V and may take U to given by Eq. (B9). Equation (B7) becomes

$$\frac{dU}{d\psi} = 2 - \frac{\epsilon H}{\rho^2} \frac{qg(-\Delta E_F - \psi)}{1+\omega^2\tau^2} ,$$

so that

$$\Delta U = 2\Delta\psi - \int_{\psi_a}^{\psi_b} \frac{\epsilon H}{\rho^2} \frac{qg}{1+\omega^2\tau^2} d\psi . \tag{B16}$$

We define

$$\alpha = \omega\tau(\psi_a) = \frac{\omega}{\nu} \exp[(\psi_a + \Delta E_F)/kT]$$

and

$$\beta = \omega\tau(\psi_b) = \frac{\omega}{\nu} \exp[(\psi_b + \Delta E_F)/kT] .$$

We integrate by parts noting that $qg\, d\psi/\rho^2 = d\rho/\rho^2$:

$$\Delta U = 2\Delta\psi + \left[\frac{\epsilon H}{\rho} \frac{1}{1+\omega^2\tau^2}\right]\Bigg|_{\psi_a}^{\psi_b} - 2\int_{\psi_a}^{\psi_b} \frac{d\psi}{1+\omega^2\tau^2} + \int_\alpha^\beta \frac{\epsilon H}{\rho} \frac{2u}{(1+u^2)^2} du$$

$$= \left[\frac{\epsilon H}{\rho} \frac{1}{1+\omega^2\tau^2}\right]\Bigg|_{\psi_a}^{\psi_b} - kT \ln\left[\frac{1+\beta^2}{1+\alpha^2}\right] + \int_\alpha^\beta \frac{\epsilon H}{\rho} \frac{2u}{(1+u^2)^2} du .$$

The function $2u/(1+u^2)^2$ is sharply peaked at $u = 1$ and has total a integrated area equal to 1. Since H and ρ are slowly varying functions, taking $\alpha << 1$ and $\beta = 1$ ($\psi_b = \psi_1$) gives

$$\Delta U = \frac{\epsilon H_1}{\rho_1} - \frac{\epsilon H_a}{\rho_a} - kT \ln 2 , \tag{B17}$$

which indicates that the correction term is roughly

$kT\ln 2$. This should be approximately doubled since we have evaluated ΔU only over $\frac{1}{2}$ of the relevant region.

How does this affect the calculated capacitance? If we call the correction factor $\delta \sim 2kT\ln 2$, then for Eq. (B12), we obtain

$$C = A\epsilon \frac{\rho_1}{\epsilon H_1^{1/2} + x_1\rho_1 - \delta\rho_1 H_1^{-1/2}} .$$

The relative error is

$$\delta(x_1 H_1^{1/2} + \epsilon H_1/\rho_1)^{-1} . \tag{B18}$$

This error is readily evaluated for the two cases presented in Sec. III A and III B. For the first case $\rho = \text{const} = q(5\times 10^{16}\ \text{cm}^{-3})$, $H_1 = 2\rho\psi_1/\epsilon$, and $\psi_1 + \Delta E_F \sim 0.5$ eV for room temperature and 10 kHz. For the depletion region formed under -5 V applied bias, $x_1 \sim 0.2$ μm. The term in parentheses is, therefore, about 2.5 V, while $\delta \sim 0.035$ eV; the discrepancy is only 1.4%.

For the second case, $g = \text{const} = 10^{17}\ \text{cm}^{-3}\,\text{eV}^{-1}$, $\rho_1 = qg\psi_1$, and $H_1 = qg\psi_1^2/\epsilon$. Again taking $\psi_1 + \Delta E_F \sim 0.5$ eV, a 5-V depletion region gives $x_1 \sim 0.3$ μm. The term in parentheses is 1.7 V; the discrepancy is 2%.

[1] A. M. Goodman, J. Appl. Phys. 34, 329 (1963).
[2] C. T. Sah and V. G. K. Reddi, IEEE Trans. Electron Devices ED-11, 345 (1964).
[3] R. R. Senechal and J. Basinski, J. Appl. Phys. 39, 3723 (1968).
[4] G. I. Roberts and C. R. Crowell, J. Appl. Phys. 41, 1767 (1970).
[5] D. L. Losee, J. Appl. Phys. 46, 2204 (1975).
[6] R. Williams, J. Appl. Phys. 37, 3411 (1966).
[7] Y. Furukawa and S. Ishibashi, Jpn. J. Appl. Phys. 5, 837 (1966); 6, 503 (1967).
[8] For a recent discussion of the application of these techniques, see Martin G. Buehler and Willie E. Phillips, Solid State Electron. 19, 777 (1976).
[9] D. V. Lang, in *Thermally Stimulated Relaxation in Solids*, Vol. 37 of *Topics in Applied Physics*, edited by P. Bräunlich (Springer, Berlin, 1979), p. 93.
[10] D. V. Lang, J. D. Cohen, and J. P. Harbison, preceding paper, Phys. Rev. B 25, 5285 (1982).
[11] M. Hirose, T. Susuki, and G. H. Döhler, Appl. Phys. Lett. 24, 234 (1979).
[12] W. E. Spear, P. G. LeComber, and A. J. Snell, Philos, Mag. B 38, 303 (1978).
[13] A. J. Snell, K. D. MacKenzie, P. G. LeCómber, and W. E. Spear, Philos. Mag. B 40, 1 (1979).
[14] P. Viktorvitch and G. Moddel, J. Appl. Phys. 51, 4847 (1980).
[15] T. Tiedje, C. R. Wronski, and J. M. Cebulka, J. Non-Cryst. Solids 35&36, 743 (1980).
[16] W. Fuhs and M. Milleville, Phys. Status Solidi B 98, K29 (1980).
[17] L. Vieus-Rochaz and A. Chenevas-Paule, J. Non-Cryst. Solids 35&36, 737 (1980).
[18] R. S. Crandall, J. Electron. Mater. 9, 713 (1980).
[19] J. D. Cohen, D. V. Lang, J. C. Bean, and J. P. Harbison, J. Non-Cryst. Solids 35&36, 581 (1980).
[20] J. D. Cohen, D. V. Lang, and J. P. Harbison, Phys. Rev. Lett. 45, 197 (1980).
[21] J. D. Cohen, D. V. Lang, J. P. Harbison, and J. C. Bean, Solar Cells 2, 331 (1980).
[22] J. Solomon, T. Dietl, and D. Kaplan, J. Phys. (Paris) 39, 1241 (1978).
[23] M. Taniellian, H. Fritzsche, C. C. Tsai, and E. Symbalisty, Appl. Phys. Lett. 33, 353 (1978).
[24] D. G. Ast and M. H. Brodsky, J. Non-Cryst. Solids 35&36, 611 (1980).
[25] The simplest example is a constant density of states which produces an exponential band-bending function (see Sec. III B). An analysis for a density of states given by hyperbolic functions has been given by M. Shur, W. Czubatyji, and A. Madan, J. Non-Cryst. Solids 35&36, 731 (1980).
[26] W. Schottky, Naturwissenschaften 26, 843 (1938).
[27] H. A. Bethe, MIT Radiation Laboratory, Report 43-12 (unpublished).
[28] See, for example, W. E. Milne, *Numerical Calculus* (Princeton University Press, Princeton, N.J., 1949), p. 140.
[29] S. M. Sze, *Physics of Semiconductor Devices* (Wiley, New York, 1969), p. 363.
[30] G. L. Miller, IEEE Trans. on Electron Devices ED-19, 1103 (1972).
[31] A. Madan, P. G. LeComber, and W. E. Spear, J. Non-Cryst. Solids 20, 239 (1976).
[32] W. E. Spear and P. G. LeComber, Solid State Commun. 17, 1193 (1976).
[33] D. V. Lang, R. A. Logan, and M. Jaros, Phys. Rev. B 19, 1015 (1979).
[34] G. D. Watkins and J. R. Troxell, Phys. Rev. Lett. 44, 593 (1980).